

UC Berkeley

UC Berkeley Previously Published Works

Title

Spin-triplet superconductivity from inter-valley Goldstone modes in magic-angle graphene

Permalink

<https://escholarship.org/uc/item/5hz9s1dp>

Authors

Kozii, Vladyslav
Zaletel, Michael P
Bultinck, Nick

Publication Date

2020-05-26

Peer reviewed

Superconductivity in a doped valley coherent insulator in magic angle graphene: Goldstone-mediated pairing and Kohn-Luttinger mechanism

Vladyslav Kozii,^{1,2} Michael P. Zaletel,^{1,2} and Nick Bultinck^{1,3}

¹*Department of Physics, University of California, Berkeley, CA 94720, USA*

²*Materials Sciences Division, Lawrence Berkeley National Laboratory, Berkeley, CA 94720, USA*

³*Department of Physics, Ghent University, 9000 Ghent, Belgium*

(Dated: May 28, 2020)

We consider magic angle graphene in the doping regime around charge neutrality and study the connection between a recently proposed intervalley coherent insulator at zero doping and the neighboring superconducting domes. The breaking of the valley $U(1)$ symmetry generates massless Goldstone modes, which couple to the doped charge carriers. We derive the effective interaction between these Goldstone modes and the conduction electrons and study its role in mediating superconductivity. Combining it with the screened Coulomb potential, we find weak-coupling superconducting instabilities in the two-component p - and d -wave channels. The competition between the two channels is set by the distance between the bilayer graphene device and the metallic gates. We find that the p -wave instability originates from the attraction mediated by the Goldstone modes, while the d -wave pairing is caused purely by the screened Coulomb interaction, similarly to the Kohn-Luttinger mechanism.

I. INTRODUCTION

The experimental discovery of superconductivity in twisted bilayer graphene (tBLG) [1] has spurred a tremendous interest to develop a theoretical understanding of the underlying pairing mechanism [2–28]. At present, the microscopic origin of superconductivity in tBLG is still under debate. For example, it is not clear whether electron pairing is the result of phonon exchange, or whether it is driven by a more exotic mechanism coming from Coulomb repulsion. It is also equally unclear whether the superconducting domes are in any way related to the correlated insulating phases which are observed in transport experiments at certain integer fillings [29–33] (signatures of these insulating phases are also seen in spectroscopic measurements [34–39]). This last question was addressed in more detail in two recent experimental works [40, 41], where superconducting domes in the doping regimes around two electrons or holes per moiré unit cell ($\nu = \pm 2$) were observed without any signature of a correlated insulator nearby. This is suggestive for the fact that the superconductors and insulators near $\nu = \pm 2$ are not related in any crucial way, and might even be competing phases.

In Refs. [31, 40] superconducting domes were also observed next to the charge neutrality point, on both the electron and hole doped sides. In Ref. [40] it was found that these domes appear only when the distance between the tBLG device and the gates is large enough, i.e., when screening by the metallic gates is sufficiently weak. This observation suggests that Coulomb repulsion plays an important role for the origin of superconductivity near charge neutrality. Interestingly, in the same devices insulating behavior is also observed at charge neutrality [31, 40] (a charge gap was also observed in the tunneling experiments of Ref. [38]).

In Ref. [42] it was proposed, based on a self-consistent

Hartree-Fock analysis, that the insulating behavior of magic angle graphene at charge neutrality is the result of an intervalley coherent order which develops at zero temperature. This type of order implies that the electron system spontaneously breaks the valley-charge conservation symmetry, and therefore has a valley Goldstone mode. The valley-coherent insulator was dubbed the K-IVC (Kramers intervalley coherent) insulator [42], because it is invariant under an emergent spinless Kramers time-reversal symmetry.

In this work, we take the K-IVC insulator of Ref. [42] as the starting point for a study of superconductivity in tBLG near charge neutrality. In particular, we investigate the potential role of the valley Goldstone mode in the formation of Cooper pairs. More concretely, we study how the attractive interaction mediated by the exchange of the Goldstone modes, taken together with the screened Coulomb interaction, can give rise to the superconducting instabilities of the doped insulator near charge neutrality. Importantly, we find that the density of states of the doped K-IVC insulator is significantly smaller than that of the “bare” (non-interacting) nearly flat bands of tBLG at the magic angle [43–45], which allows us to treat the problem within a weak-coupling approach. We note that the role of valley Goldstone modes for superconductivity has also been discussed previously in Ref. [46], where the authors considered a phenomenological inter-valley coherent insulator in tBLG.

Remarkably, we find that the leading superconducting instability in the doped K-IVC state is either in the two-component p -wave or d -wave channel, depending on the gate distance. The origin of this result is rooted in the interplay between the attraction mediated by the Goldstone modes and screened Coulomb interaction. When the distance between the gates is sufficiently large and the K-IVC state is well-developed, the interaction due to Goldstone modes has sufficiently strong components in both s -wave and p -wave channels. The former, how-

ever, is significantly suppressed by the repulsive part of the Coulomb interaction, resulting in p -wave superconductivity. The d -wave pairing state, on the other hand, originates purely from the Coulomb interaction, similarly to the Kohn-Luttinger mechanism [47, 48]. The momentum-dependent screening due to the doped charge carriers generates strong attractive component in the d -wave channel, which becomes dominant when the distance between the gates becomes small enough. Finally, we emphasize that our results do not rely on the retardation effects that are required to weaken strong Coulomb repulsion in conventional metals. The absence of retardation generally poses a serious problem in the study of superconductivity in low-density materials with a small Fermi energy [49–51], but does not play a significant role in our work.

Our BCS-type calculation predicts the value of the dimensionless interaction strength in the Cooper channel of approximately $\lambda \approx 0.1$ for both p -wave and d -wave channels. This is an unexpectedly large value for the d -wave pairing realized through the Kohn-Luttinger mechanism, which is usually believed to be extremely weak [47]. However, this value is still too small to explain the experimentally observed superconducting transition temperature $T_c \approx 0.3$ K. Nevertheless, since T_c is exponentially sensitive to λ , $T_c \propto \exp(-1/\lambda)$, one would obtain the value of T_c comparable to the experiment if λ is only two times larger. One way to obtain a larger value of λ is to take the electron's mass renormalization into account, which has been neglected in this work. The enhanced effective mass would increase density of states at the Fermi level, leading to a higher value of λ . We leave the detailed study of this and related questions for a future work.

As was found in Ref. [42], the valley coherent order at charge neutrality gets destroyed under sufficient substrate alignment. The pairing instabilities discussed in the present work would then disappear together with it. This could potentially explain why no superconductivity is seen in the aligned devices of Refs. [32, 33]. As explained in more detail below, the pairing instabilities we find are also sensitive to the gate distance, which could explain the correlation between gate distance and critical temperature observed in Ref. [40].

We want to point out that a recent work has put forward another, topological pairing mechanism for superconductivity in tBLG, also starting from the same K-IVC insulator at charge neutrality. In Ref. [28], the analogy between tBLG at charge neutrality and two time-reversed copies of a quantum Hall ferromagnet was used to propose that superconductivity results from the condensation of charge- $2e$ skyrmions. It was found [28] that these skyrmion excitations become energetically competitive with the conventional electron excitations at small doping. It is not clear whether the topological pairing mechanism of Ref. [28] is in any way competing with the Fermi surface instabilities discussed in this work. And if they were to be competing mechanisms, then the compe-

tion is likely to be set by microscopic details which are highly sample-dependent.

The remainder of the paper is organized as follows. In Sec. II, we start by reviewing the essential properties of the valley-coherent insulator found in Ref. [42]. In Sec. III, we derive the coupling between electrons in the conduction bands of the valley-coherent state and the valley Goldstone mode (for concreteness, we focus on electron doping). In Sec. IV, we briefly discuss the repulsive Coulomb interaction between the doped electrons and how it gets screened in the conventional way by particle-hole excitations. The effective attractive and repulsive interactions for electrons at the Fermi surface are discussed in Sec. V. In the same section, we also decompose the interaction in the different angular momentum channels and look for superconducting instabilities. We end with a discussion and outlook in Sec. VI. In the Appendices, we provide additional details on how to calculate the Goldstone mode propagator at charge neutrality and on how to derive an effective low-energy theory for the doped electron system and the Goldstone modes. We also give a more thorough discussion of the analysis of the superconducting instabilities.

II. THE K-IVC INSULATOR AT CHARGE NEUTRALITY

Our starting point is the Kramers intervalley coherent (K-IVC) insulator, which was proposed in Ref. [42] to describe the ground state of magic angle graphene at charge neutrality (we note that similar states were also discussed previously in Refs. [46, 52]). More recently, evidence for intervalley coherence in tBLG at charge neutrality was also found in a quantum Monte Carlo study [53]. We write the mean-field Hamiltonian of the K-IVC insulator as

$$H = H_0 + H_\Delta = \sum_{\mathbf{k}} c_{\mathbf{k}}^\dagger [h_0(\mathbf{k}) + \Delta(\mathbf{k})] c_{\mathbf{k}}, \quad (1)$$

where H_0 is the valley-symmetric part and H_Δ is the order parameter contribution. By definition, the order parameter satisfies $\tau_z \Delta(\mathbf{k}) \tau_z = -\Delta(\mathbf{k})$, where τ_z is the third Pauli matrix acting on the valley indices. The electron operators $c_{\mathbf{k}}^\dagger$ are defined in the band basis of the Bistritzer-MacDonald (BM) model of twisted bilayer graphene [45]. This means that each electron carries valley and spin quantum numbers $\tau \in \{+, -\}$ and $s \in \{\uparrow, \downarrow\}$, along with a BM band label a . For our numerical simulations, we keep six bands per spin and valley, corresponding to the two flat bands and the first two dispersive bands above and below charge neutrality. The order parameter contribution H_Δ breaks both the valley $U(1)$ symmetry [denoted as $U_V(1)$] and spinless time-reversal symmetry \mathcal{T} [42], which act as

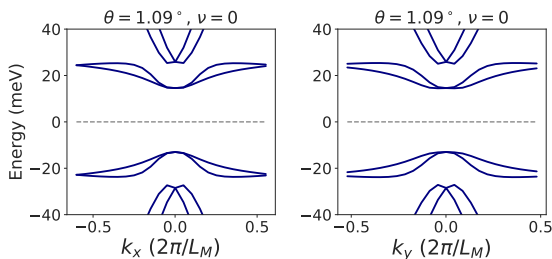


FIG. 1. Self-consistent mean-field band structure of the K-IVC state at charge neutrality along two cuts through the mini-BZ, one in the x -direction (left panel) and one in the y -direction (right panel). The parameters which were used in the BM Hamiltonian are $w_1 = 110$ meV and $w_0/w_1 = 0.75$, where w_0 (w_1) is the sublattice diagonal (off-diagonal) interlayer tunneling strength. For the interaction, a dual-gate screened Coulomb interaction with gate distance $D = 15$ nm and dielectric constant $\epsilon = 10$ was used. For more details, see Ref. [42].

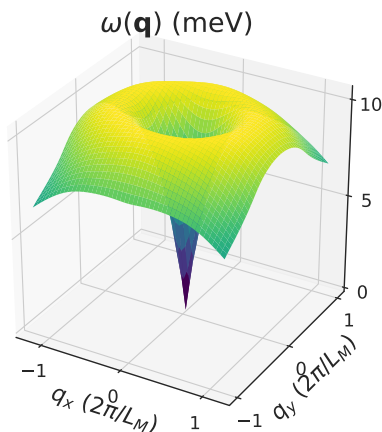


FIG. 2. Dispersion of the K-IVC Goldstone mode at charge neutrality.

$$U_V(1) : c_{\tau,s,a,\mathbf{k}}^\dagger \rightarrow e^{i\tau\phi} c_{\tau,s,a,\mathbf{k}}^\dagger, \quad (2)$$

$$\mathcal{T} : c_{\tau,s,a,\mathbf{k}}^\dagger \rightarrow c_{-\tau,s,a,-\mathbf{k}}^\dagger, \quad i \rightarrow -i. \quad (3)$$

In Fig. 1, the band structure of the K-IVC insulator is shown along two orthogonal cuts through the mini-Brillouin zone (mini-BZ). Although the K-IVC state breaks both time-reversal and $U_V(1)$, it preserves an emergent Kramers time-reversal symmetry $\tilde{\mathcal{T}} = \tau_z \mathcal{T} = i\tau_y K$ [42], where τ_i are the Pauli matrices acting on the valley indices and K is complex conjugation. Because of this Kramers time-reversal symmetry, the K-IVC band structure has, on top of the spin degeneracy, an additional two-fold Kramers degeneracy at the Γ and the M points, i.e., the time-reversal invariant points in the mini-BZ.

Because the $U_V(1)$ symmetry is broken spontaneously, there is a Goldstone mode at zero temperature. In reality,

the $U_V(1)$ symmetry is weakly broken, so the Goldstone modes will acquire a small mass. Here, however, we ignore these very small $U_V(1)$ symmetry breaking terms and derive the leading (quadratic) terms in the effective action of the Goldstone modes by integrating out the gapped fermions. The resulting imaginary time action then takes the general form

$$S_G = -\frac{1}{2} \int \frac{d\omega}{2\pi} \int \frac{d\mathbf{q}}{(2\pi)^2} \phi(i\omega, \mathbf{q}) D^{-1}(i\omega, \mathbf{q}) \phi(-i\omega, -\mathbf{q}), \quad (4)$$

with

$$D^{-1}(i\omega, \mathbf{q}) = \chi_s(i\omega)^2 - K(\mathbf{q}). \quad (5)$$

In Appendices A and B, it is explained how we compute both $K(\mathbf{q})$ and χ_s from the mean-field K-IVC band structure. From the long wavelength part of $K(\mathbf{q})$, one obtains the stiffness of the K-IVC state ρ_s as $K(\mathbf{q}) = \rho_s \mathbf{q}^2 + \mathcal{O}(\mathbf{q}^4)$. We find numerically that $\rho_s \approx 4$ meV, which agrees with the value obtained in Ref. [28] via a different method. For χ_s , we find numerical values $\chi_s \approx 0.1$ meV $^{-1} L_M^{-2}$ (in units where $\hbar = 1$), with $L_M \approx 12$ nm the moiré lattice constant at the magic angle. The Goldstone mode velocity v_G is given by

$$v_G = \sqrt{\frac{\rho_s}{\chi_s}}, \quad (6)$$

and is of the order $v_G \approx 6.3$ meV $\times L_M$. From Eq. (4), we also obtain the Goldstone mode dispersion $\omega(\mathbf{q})$ as

$$\omega(\mathbf{q}) = \sqrt{\frac{K(\mathbf{q})}{\chi_s}}. \quad (7)$$

In Fig. 2, we plot $\omega(\mathbf{q})$ for values of $\mathbf{q} \lesssim 2\pi/L_M$. Note that $\phi(\tau, \mathbf{r})$ is a continuum field, and that its dispersion is not periodic under shifts by moiré reciprocal lattice vectors. From Fig. 2, we see that $\omega(\mathbf{q})$ reaches a maximal value of ≈ 10 meV when $|\mathbf{q}| \sim \pi/L_M$, and starts decaying for larger momenta.

III. DOPING THE K-IVC STATE AND COUPLING TO GOLDSTONE MODES

In this section, we consider what happens if we dope away from the charge neutrality point. For concreteness, we focus on electron doping and work at a filling $\nu = 1/4$ (i.e., one electron for every four moiré unit cells). By solving the Hartree-Fock self-consistency equations at $\nu = 1/4$, we find that the K-IVC bands do not change significantly compared to those at charge neutrality. The additional doped electrons simply occupy the lowest-energy states in the conduction bands of the

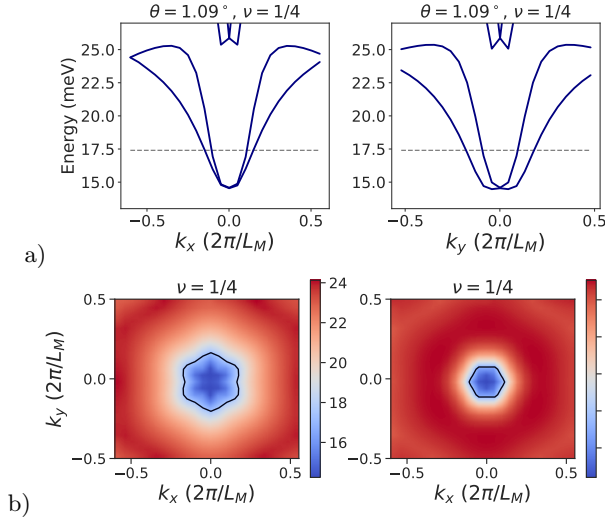


FIG. 3. (a) K-IVC conduction bands at $\theta = 1.09^\circ$ with the Fermi energy at $\nu = 1/4$ indicated by a gray dashed line. (b) Colorplots of the band energies of the two K-IVC conduction bands with a contour corresponding to the two Fermi pockets around Γ at $\nu = 1/4$.

band structure at charge neutrality, without any major changes to the dispersion or the energy gap between valence and conduction bands. In Fig. 3, the K-IVC conduction bands are shown and the Fermi energy at $\nu = 1/4$ is indicated by a gray dashed line. It lies approximately 3.2 meV above the conduction band minimum. From Fig. 3, we see that at $\nu = 1/4$ there are two Fermi surfaces around the Γ point. The average Fermi velocity for electrons at the outer (inner) Fermi surface is $v_{F,1} \approx 5.5 \text{ meV} \times L_M$ ($v_{F,2} \approx 8 \text{ meV} \times L_M$). Throughout this work, we will use a notation where subscript 1 (2) refers to the lower (upper) K-IVC conduction band containing the outer (inner) Fermi surface. In Fig. 4, we show the Fermi energy ε_F and the density of states at the Fermi energy $N(0)$ as a function of the filling ν . We see that for $\nu = 1/4$, the density of states is given by $N(0) \approx 0.08 \text{ meV}^{-1} L_M^{-2}$. Note that this value is significantly smaller than the density of states in the BM bands at the magic angle, where the density of states is $N(0)_{BM} \gtrsim 1 \text{ meV}^{-1} L_M^{-2}$. This will be important for our analysis below.

We now derive the coupling between the electrons in the conduction bands and the K-IVC Goldstone modes. Similarly to the calculation of $K(\mathbf{q})$ in Appendix A, we start from the Hamiltonian [54]

$$H[\phi] = H_0 + e^{-i\hat{Q}} H_\Delta e^{i\hat{Q}}, \quad (8)$$

where

$$\hat{Q} = \frac{1}{2} \int d\mathbf{r} \phi(\mathbf{r}) f_{\mathbf{r}}^\dagger \tau_z f_{\mathbf{r}} \quad (9)$$

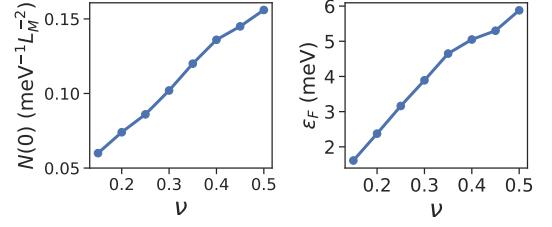


FIG. 4. Density of states at the Fermi energy $N(0)$ and the Fermi energy ε_F (relative to the band minimum) of the K-IVC conduction bands as a function of the filling factor ν .

is the operator that generates spatially-dependent valley rotations. Specifically, the function $\phi(\mathbf{r})$ is the spatially-dependent $U_V(1)$ angle over which the K-IVC order parameter is rotated and $f_{\mathbf{r}}^\dagger$ are the real-space fermion creation operators of the tBLG continuum model [43–45] in the orbital basis. Going to momentum space and transforming to the band basis of the BM model we can write \hat{Q} as

$$\hat{Q} = \frac{1}{2\sqrt{A}} \sum_{\mathbf{k}, \mathbf{q}} \phi_{\mathbf{q}} c_{\mathbf{k}+\mathbf{q}}^\dagger \Lambda_{\mathbf{q}}(\mathbf{k}) \tau_z c_{\mathbf{k}}, \quad (10)$$

where A is the area of the system and $c_{m,\mathbf{k}}^\dagger$ create electrons in the BM bands, with $m = (\tau, s, a)$ a combined valley, spin, and band index. The sum over \mathbf{k} is restricted to the first mini-BZ, while the sum over \mathbf{q} runs over all BZ in the repeated zone scheme. In Eq. (10), the form factors $\Lambda_{\mathbf{q}}(\mathbf{k})$ result from doing the unitary transformation from the orbital basis to the BM band basis and they are defined as

$$[\Lambda_{\mathbf{q}}(\mathbf{k})]_{mn} = \langle v_{m,\mathbf{k}+\mathbf{q}} | v_{n,\mathbf{k}} \rangle, \quad (11)$$

where $|v_{m,\mathbf{k}}\rangle$ are the periodic part of the Bloch states of the BM Hamiltonian. Note that since the BM bands have a well-defined valley quantum number, we could put the valley matrix τ_z outside of the form factor in Eq. (10).

Expanding $H[\phi]$ to first order in ϕ we find

$$H[\phi] = H - i[\hat{Q}, H_\Delta], \quad (12)$$

where $H = \sum_{\mathbf{k}} c_{\mathbf{k}}^\dagger [h_0(\mathbf{k}) + \Delta(\mathbf{k})] c_{\mathbf{k}}$ is the K-IVC mean-field Hamiltonian. Written out explicitly, the first order term takes the form

$$-i[\hat{Q}, H_\Delta] = \frac{i}{2\sqrt{A}} \sum_{\mathbf{k}, \mathbf{q}} \phi_{\mathbf{q}} c_{\mathbf{k}+\mathbf{q}}^\dagger [\Delta(\mathbf{k} + \mathbf{q}) \Lambda_{\mathbf{q}}(\mathbf{k}) \tau_z - \Lambda_{\mathbf{q}}(\mathbf{k}) \tau_z \Delta(\mathbf{k})] c_{\mathbf{k}}. \quad (13)$$

We now perform a transformation to the eigenbasis of the K-IVC Hamiltonian, where $H =$

$\sum_{\alpha,s,\mathbf{k}} E_{\alpha,\mathbf{k}} \psi_{\alpha,s,\mathbf{k}}^\dagger \psi_{\alpha,s,\mathbf{k}}$. The electron operators $\psi_{\alpha,s,\mathbf{k}}^\dagger$, labeled by a K-IVC band index α and a spin index s , are related to the electron operators in the BM basis as

$$\psi_{\alpha,s,\mathbf{k}}^\dagger = \sum_m [u_{\alpha,\mathbf{k}}]_m c_{m,s,\mathbf{k}}^\dagger, \quad (14)$$

where $[u_{\alpha,\mathbf{k}}]_m$ are the components of the K-IVC eigenstates $|u_{\alpha,\mathbf{k}}\rangle$. In the K-IVC eigenbasis, the first order term in ϕ takes the form

$$-i[\hat{Q}, H_\Delta] = \frac{1}{\sqrt{A}} \sum_{\mathbf{k},\mathbf{q}} \sum_{\alpha,\beta,s} g_{\alpha\beta}(\mathbf{k},\mathbf{q}) \phi_{\mathbf{q}} \psi_{\alpha,s,\mathbf{k}+\mathbf{q}}^\dagger \psi_{\beta,s,\mathbf{k}}, \quad (15)$$

where the electron-boson coupling $g_{\alpha\beta}(\mathbf{k},\mathbf{q})$ is given by

$$g_{\alpha\beta}(\mathbf{k},\mathbf{q}) = \frac{i}{2} \langle u_{\alpha,\mathbf{k}+\mathbf{q}} | (\Delta(\mathbf{k}+\mathbf{q}) \Lambda_{\mathbf{q}}(\mathbf{k}) \tau_z - \tau_z \Lambda_{\mathbf{q}}(\mathbf{k}) \Delta(\mathbf{k})) | u_{\beta,\mathbf{k}} \rangle. \quad (16)$$

From $\Lambda_0(\mathbf{k}) = \mathbf{1}$, we see that the coupling at zero momentum transfer can be written as [54]

$$\begin{aligned} g_{\alpha\beta}(\mathbf{k}, 0) &= \frac{i}{2} \langle u_{\alpha,\mathbf{k}} | [\Delta(\mathbf{k}), \tau_z] | u_{\beta,\mathbf{k}} \rangle \\ &= \frac{i}{2} \langle u_{\alpha,\mathbf{k}} | \tau_z | u_{\beta,\mathbf{k}} \rangle \times (E_{\alpha,\mathbf{k}} - E_{\beta,\mathbf{k}}), \end{aligned} \quad (17)$$

where we have used that $[\Delta(\mathbf{k}), \tau_z] = [h_0(\mathbf{k}) + \Delta(\mathbf{k}), \tau_z]$. Written in this form, it is clear that the intraband scattering processes vanish at zero momentum transfer. This important property implies that, at small coupling, the Goldstone modes are not Landau damped and do not destroy the Landau quasi-particles [54].

The coupling of the electrons to the Goldstone modes will lead to an effective attractive interaction between the electrons, similar to the attractive interaction mediated by acoustic phonons. Below, we will investigate the potential role of this attractive interaction for superconductivity. But before doing so, we first discuss the repulsive Coulomb interaction in the next section.

IV. COULOMB INTERACTION AND SCREENING

The bare repulsive interaction between the doped electrons in the K-IVC conduction bands is given by

$$H_C = \frac{1}{2A} \sum_{\mathbf{q}} V_C(q) : \rho_{\mathbf{q}} \rho_{-\mathbf{q}} :, \quad (18)$$

where $V_C(q)$ the dual gate-screened Coulomb potential

$$V_C(q) = \frac{e^2}{2\epsilon_0\epsilon} \frac{\tanh(Dq)}{q}. \quad (19)$$

In this expression, D is the distance from the tBLG device to the metallic gates and ϵ is the dielectric constant. Note that in the Coulomb interaction, the sum over \mathbf{q} is not restricted to the first mini-BZ, but goes over all BZ in the repeated zone scheme. The operators $\rho_{\mathbf{q}}$ are defined as

$$\rho_{\mathbf{q}} = \sum_{\mathbf{k}} \psi_{\mathbf{k}+\mathbf{q}}^\dagger F_{\mathbf{q}}(\mathbf{k}) \psi_{\mathbf{k}} \quad (20)$$

and correspond to the density of electrons in the K-IVC conduction bands. The form factors $F_{\mathbf{q}}(\mathbf{k})$ which appear in this expression are given by

$$[F_{\mathbf{q}}(\mathbf{k})]_{\alpha\beta} = \langle u_{\alpha,\mathbf{k}+\mathbf{q}} | \Lambda_{\mathbf{q}}(\mathbf{k}) | u_{\beta,\mathbf{k}} \rangle, \quad (21)$$

where $|u_{\alpha,\mathbf{k}}\rangle$ are the K-IVC eigenstates corresponding to the conduction bands and $\Lambda_{\mathbf{q}}(\mathbf{k})$ are the form factors defined previously in Eq. (11). The form factors $\Lambda_{\mathbf{q}}(\mathbf{k})$ result from expressing the Coulomb interaction in the BM band basis (see, e.g., Ref. [42] for details). Note that because of these form factors the Coulomb interaction acquires an explicit dependence on the incoming momenta \mathbf{k} and \mathbf{k}' .

Because there is a Fermi surface at $\nu = 1/4$, the electrons can efficiently screen the Coulomb interaction. To take this effect into account, we calculate the standard (static) polarization bubble, which evaluates to

$$\Pi(\mathbf{q}) = -2 \int \frac{d\mathbf{k}}{(2\pi)^2} \sum_{\alpha,\beta} \frac{n_{\alpha,\mathbf{k}+\mathbf{q}} - n_{\beta,\mathbf{k}}}{E_{\alpha,\mathbf{k}+\mathbf{q}} - E_{\beta,\mathbf{k}}} |[F_{\mathbf{q}}(\mathbf{k})]_{\alpha\beta}|^2, \quad (22)$$

where $n_{\alpha,\mathbf{k}} = n(E_{\alpha,\mathbf{k}}) = \Theta(\varepsilon_F - E_{\alpha,\mathbf{k}})$ is the zero-temperature Fermi-Dirac distribution [$\Theta(x)$ is the Heaviside step function] representing the fermion occupation numbers, ε_F is the Fermi energy, and the factor of two comes from the spin degeneracy.

From the polarization bubble we obtain the dielectric function $\epsilon(\mathbf{q}) = 1 + V_C(q)\Pi(\mathbf{q})$, which appears in the static RPA screened Coulomb interaction

$$\begin{aligned} V_{\alpha\beta\lambda\sigma}^{C,scr}(\mathbf{q}, \mathbf{k}, \mathbf{k}') &= \frac{V_C(q)}{\epsilon(\mathbf{q})} [F_{\mathbf{q}}(\mathbf{k})]_{\alpha\beta} [F_{-\mathbf{q}}(\mathbf{k}')]_{\lambda\sigma} \\ &= \frac{e^2}{2\epsilon_0\epsilon} \frac{\tanh(Dq)}{q + k_s(\mathbf{q})} [F_{\mathbf{q}}(\mathbf{k})]_{\alpha\beta} [F_{-\mathbf{q}}(\mathbf{k}')]_{\lambda\sigma}. \end{aligned} \quad (23)$$

In the last line, we have defined a \mathbf{q} -dependent inverse screening length $k_s(\mathbf{q})$ given by

$$k_s(\mathbf{q}) = \frac{e^2}{2\epsilon_0\epsilon} \Pi(\mathbf{q}) \tanh(Dq). \quad (24)$$

In Fig. 5, the inverse screening length $k_s(\mathbf{q})$ is plotted, both in the \mathbf{q} -plane and along the two cuts in the q_x - and q_y -directions. We see that $k_s(\mathbf{q})$ decays as a function of $|\mathbf{q}|$ and becomes negligibly small when $|\mathbf{q}| \sim 4\pi/L_M$. This is a result of the decay of the form factors $F_{\mathbf{q}}(\mathbf{k})$.

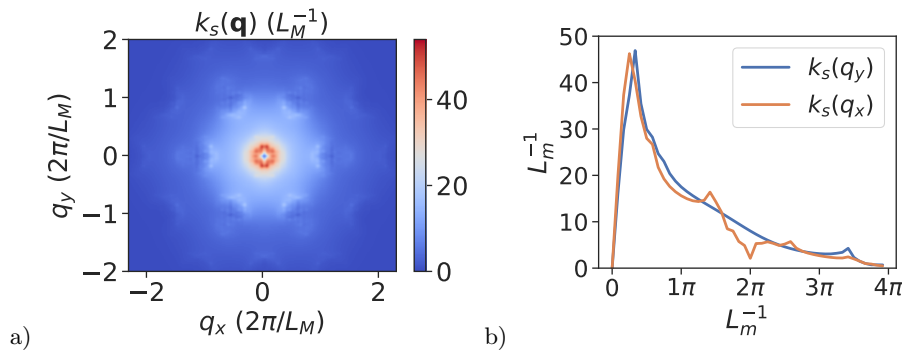


FIG. 5. (a) Inverse screening length $k_s(\mathbf{q})$ as a function of \mathbf{q} . (b) Inverse screening length $k_s(\mathbf{q})$ along a cut in the q_x - and q_y -directions. The results were obtained at filling $\nu = 1/4$ on a 24×24 momentum grid using $\theta = 1.09^\circ$, $\epsilon = 10$, and $D = 15$ nm.

V. INTERACTIONS IN THE COOPER CHANNEL AND SUPERCONDUCTING INSTABILITIES

In this Section, we examine both the screened Coulomb interaction and the Goldstone mode-mediated interaction in the Cooper channel to perform the standard BCS-type analysis of superconductivity. The screened Coulomb interaction $V_{\alpha\beta\lambda\sigma}^{C,scr}(\mathbf{q}, \mathbf{k}, \mathbf{k}')$ was defined previously in Eq. (23). As for the attractive interaction mediated by the Goldstone modes, we find that it is given by

$$H_G = \frac{1}{2A} \sum_{\mathbf{q}, \mathbf{k}, \mathbf{k}'} V_{\alpha\beta\lambda\sigma}^G(\mathbf{q}, \mathbf{k}, \mathbf{k}') \times \psi_{\alpha,s,\mathbf{k}+\mathbf{q}}^\dagger \psi_{\lambda,s',\mathbf{k}'-\mathbf{q}}^\dagger \psi_{\sigma,s',\mathbf{k}'} \psi_{\beta,s,\mathbf{k}}, \quad (25)$$

where the summation over band indices $\alpha, \beta, \lambda, \sigma$ and spin indices s, s' is implicit. Note that similarly to the Coulomb interaction the sum over \mathbf{q} in Eq. (25) runs over all mini-BZ in the repeated zone scheme. The potential $V^G(\mathbf{q}, \mathbf{k}, \mathbf{k}')$ is given by

$$V_{\alpha\beta\lambda\sigma}^G(\mathbf{q}, \mathbf{k}, \mathbf{k}') = g_{\alpha\beta}(\mathbf{k}, \mathbf{q}) D(0, \mathbf{q}) g_{\lambda\sigma}(\mathbf{k}', -\mathbf{q}), \quad (26)$$

where $D(0, \mathbf{q}) = -K(\mathbf{q})^{-1}$ is the Goldstone mode propagator defined in Eq. (5) evaluated at zero frequency and $g_{\alpha\beta}(\mathbf{k}, \mathbf{q})$ is the coupling function defined in Eq. (16).

The fact that the interaction mediated by the Goldstone mode at charge neutrality and at finite doping have approximately the same form, Eq. (25), is a non-trivial result. We discuss it in detail in Appendix C, where we use the path-integral formalism to integrate out the valence band fermionic degrees of freedom and derive the effective low-energy theory that couples Goldstone modes and the conduction band fermions. After carefully summing up certain sets of diagrams we end up with the conclusion that, to good accuracy, the effective

interaction between the electrons on the Fermi surface mediated by Goldstone modes is given by the same expression that one would obtain by integrating out Goldstone modes at charge neutrality, i.e., Eqs. (25)-(26). We emphasize that this interaction should not be viewed as some low-energy starting point that need to be further renormalized by, e.g., particle-hole modes. Instead, it is an effective interaction that already takes into account important renormalization effects and will be used directly to calculate superconducting instabilities. This is somewhat similar in spirit to the Eliashberg theory of superconductivity, where one self-consistently solves for the electron Green's function, while taking electron-phonon interaction as an input parameter (we, however, do not study the frequency dependence of the gap function in this paper, but do a BCS-type analysis instead). Another important result that we obtain and discuss in detail in Appendix C is that the Goldstone mode-mediated attraction (25) is very weakly screened by the Coulomb interaction.

From Fig. 4, we see that for filling factors $0 < \nu < 0.5$, the Fermi energy is smaller than the Goldstone mode bandwidth, which we previously established to be around 10 meV. This implies that we cannot invoke retardation effects to decrease the Coulomb pseudopotential. We therefore inevitably arrive at the conclusion that to obtain conventional s -wave superconductivity purely from the Goldstone mode exchange we need an attractive interaction which is larger than the repulsive Coulomb interaction. This seems hard to achieve, which motivates us to also explore higher-harmonics superconducting channels.

To study the superconducting instabilities, we focus on the Cooper channel of the effective interaction given by the sum of Eqs. (23) and (25):

$$\hat{V}_{\alpha\beta}^C(\mathbf{k}', \mathbf{k}) = \sum_{\mathbf{G}} V_{\alpha\beta\alpha\beta}^{C,scr}(\mathbf{k}' - \mathbf{k} + \mathbf{G}, \mathbf{k}, -\mathbf{k}), \quad (27)$$

$$\hat{V}_{\alpha\beta}^G(\mathbf{k}', \mathbf{k}) = \sum_{\mathbf{G}} V_{\alpha\beta\alpha\beta}^G(0, \mathbf{k}' - \mathbf{k} + \mathbf{G}, \mathbf{k}, -\mathbf{k}), \quad (28)$$

where the sum over moiré reciprocal lattice vectors \mathbf{G} takes into account the umklapp process due to the superlattice potential. In our numerical calculations, we restrict \mathbf{G} to lie within the first three shells of mini-BZ.

$$\hat{V}_{\alpha\beta}^C(\mathbf{k}', \mathbf{k}) = e^{i\varphi_\alpha(\mathbf{k}')} \left(\sum_{\mathbf{G}} \frac{V_C(|\mathbf{k}' - \mathbf{k} + \mathbf{G}|)}{\epsilon(\mathbf{k}' - \mathbf{k} + \mathbf{G})} | [F_{\mathbf{k}' - \mathbf{k} + \mathbf{G}}(\mathbf{k})]_{\alpha\beta} |^2 \right) e^{-i\varphi_\beta(\mathbf{k})}, \quad (29)$$

$$\hat{V}_{\alpha\beta}^G(\mathbf{k}', \mathbf{k}) = e^{i\varphi_\alpha(\mathbf{k}')} \left(\sum_{\mathbf{G}} D(0, \mathbf{k}' - \mathbf{k} + \mathbf{G}) |g_{\alpha\beta}(\mathbf{k}, \mathbf{k}' - \mathbf{k} + \mathbf{G})|^2 \right) e^{-i\varphi_\beta(\mathbf{k})}, \quad (30)$$

where $e^{i\varphi_\alpha(\mathbf{k}')}$ and $e^{-i\varphi_\beta(\mathbf{k})}$ are gauge-dependent phase factors. These phase factors do not play an important role in our analysis of the superconducting instabilities and we can simply omit them for now. At the end of our discussion, we will reintroduce these phase factors.

Next, we define the total interaction potential in the Cooper channel for electrons on the Fermi surface as

$$V_{\alpha\beta}(\theta', \theta) = \hat{V}_{\alpha\beta}^C[\mathbf{k}_{F,\alpha}(\theta'), \mathbf{k}_{F,\beta}(\theta)] + \hat{V}_{\alpha\beta}^G[\mathbf{k}_{F,\alpha}(\theta'), \mathbf{k}_{F,\beta}(\theta)], \quad (31)$$

where θ and θ' are polar angles in momentum space and $\mathbf{k}_{F,\alpha}(\theta)$ is the (angle-dependent) Fermi momentum on the Fermi surface of band α .

We will look for superconducting instabilities with gap functions of the form

$$\tilde{\Delta}_{\mathbf{k}}^s = \begin{pmatrix} \tilde{\Delta}_{1,\mathbf{k}} & 0 \\ 0 & \tilde{\Delta}_{2,\mathbf{k}} \end{pmatrix} \otimes is_y, \quad (32)$$

$$\tilde{\Delta}_{\mathbf{k}}^t = \begin{pmatrix} \tilde{\Delta}_{1,\mathbf{k}} & 0 \\ 0 & \tilde{\Delta}_{2,\mathbf{k}} \end{pmatrix} \otimes is_y \mathbf{s}, \quad (33)$$

where $\tilde{\Delta}_{\mathbf{k}}^s$ and $\tilde{\Delta}_{\mathbf{k}}^t$ correspond to spin-singlet and spin-triplet gaps, respectively, and $\tilde{\Delta}_{\alpha,\mathbf{k}}$ (or $\tilde{\Delta}_{\alpha,\mathbf{k}}$) is the gap function in the band labeled by α . Note that we use a tilde to distinguish the superconducting gap from the K-IVC order parameter.

As reviewed in more detail in Appendix E, to find superconducting instabilities with gaps as in Eqs. (32) and (33) we need to solve the following eigenvalue equation [55]

$$\sum_{\beta} \int \frac{d\theta}{2\pi} V_{\alpha\beta}(\theta', \theta) N_{\beta}(0) \tilde{\Delta}_{\beta}(\theta) = -\lambda \tilde{\Delta}_{\alpha}(\theta'), \quad (34)$$

where $\lambda > 0$ and $N_{\beta}(0)$ is the density of states per spin at Fermi surface β , which is given by

$$N_{\beta}(0) = \int \frac{d\theta}{2\pi} \frac{k_{F,\beta}(\theta)}{2\pi} \left| \frac{\partial E_{\beta}(k, \theta)}{\partial k} \right|_{k=k_{F,\beta}(\theta)}^{-1}. \quad (35)$$

In Appendix D, it is shown that because of the Kramers time-reversal symmetry of the K-IVC state, the interactions in the Cooper channel can be written as

Note that $N_1(0) + N_2(0) = N(0)/2$, since we previously defined $N(0)$ to contain a spin degeneracy factor. While Eq. (34) is written for the spin-singlet gap function, equation for the spin-triplet pairing has exactly same form with $\tilde{\Delta}_{\alpha(\beta)}$ being replaced with $\tilde{\Delta}_{\alpha(\beta)}$.

To find the solutions of Eq. (34), we go to the angular momentum basis and define

$$V_{\alpha\beta}(m, n) = \int \frac{d\theta'}{2\pi} \int \frac{d\theta}{2\pi} e^{im\theta'} V_{\alpha\beta}(\theta', \theta) e^{-in\theta}. \quad (36)$$

Because $V_{\alpha\beta}(m, n)$ is real (recall that we ignore the gauge-dependent phase factors for now), it follows that $V_{\alpha\beta}^*(m, n) = V_{\alpha\beta}(-m, -n)$. Also, because the K-IVC state is invariant under the mirror symmetry $(x, y) \rightarrow (x, -y)$, it follows that $V_{\alpha\beta}(-\theta', -\theta) = V_{\alpha\beta}(\theta', \theta)$. This implies that $V_{\alpha\beta}(m, n) = V_{\alpha\beta}(-m, -n) = V_{\alpha\beta}^*(m, n)$, such that that the components $V_{\alpha\beta}(m, n)$ are real. And finally, since the K-IVC state is invariant under six-fold rotations, it also follows that $V_{\alpha\beta}(m, n) = 0$ if $m \neq n \pmod{6}$.

For the numerical calculations, we restrict ourselves to angular harmonics $e^{in\theta}$ with $|n| \leq 6$. This converts the eigenvalue equation (34) to a set of decoupled finite-dimensional matrix eigenvalue equations

$$\sum_{\beta, M} V_{\alpha\beta}(n+6N, n+6M) N_{\beta}(0) \tilde{\Delta}_{\beta, M}^n = -\lambda_n \tilde{\Delta}_{\alpha, N}^n, \quad (37)$$

labeled by $n \in \{0, \pm 1, \pm 2, 3\}$. In Eq. (37), we have defined $\tilde{\Delta}_{\alpha, N}^n \equiv \tilde{\Delta}_{\alpha, n+6N}$, and $\tilde{\Delta}_{\alpha, n} = \int \frac{d\theta}{2\pi} e^{in\theta} \tilde{\Delta}_{\alpha}(\theta)$. Numerically, the summation over M is restricted by the requirement that $|n+6M| \leq 6$ (same holds for N , i.e., $|n+6N| \leq 6$). Solutions to Eq. (37) with $n = 0$ describe instabilities in the s -wave channel, solutions with $n = \pm 1$ are instabilities in the degenerate p -wave channels, $n = \pm 2$ correspond to the degenerate d -wave channels, and $n = 3$ is the f -wave channel. Of course, solutions with even (odd) angular momentum necessarily correspond to spin-singlet (spin-triplet) gaps.

The gap functions on the Fermi surfaces corresponding to the different λ_n are determined by the eigenvectors $\tilde{\Delta}_{\alpha, N}^n$:

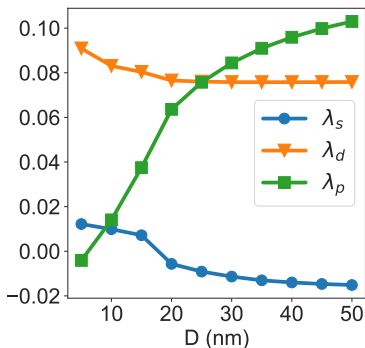


FIG. 6. Dimensionless interaction strengths of the superconducting s -, p -, and d -wave channels as a function of the gate distance D .

$$\tilde{\Delta}_\alpha^n(\theta) = \sum_N \tilde{\Delta}_{\alpha,N}^n e^{-i(n+6N)\theta}. \quad (38)$$

At this point, it is straightforward to reintroduce the gauge-dependent phase factors $e^{i\varphi_\alpha(\theta)}$. One finds that these phase factors do not change the values of λ_n , but only modify the gap function to take the form

$$\tilde{\Delta}_\alpha^n(\theta) = e^{i\varphi_\alpha(\theta)} \sum_N \tilde{\Delta}_{\alpha,N}^n e^{-i(n+6N)\theta} \quad (39)$$

In Fig. 6, we plot the numerically obtained values for λ_s , λ_p , and λ_d as a function of gate distance D . We omit λ_f since we do not find a non-trivial solution for the gap equation in this channel. The results in Fig. 6 were obtained using $N_1(0) = 2.9 \times 10^{-2} \text{ meV}^{-1} L_M^{-2}$ and $N_2(0) = 1.1 \times 10^{-2} \text{ meV}^{-1} L_M^{-2}$.

We see that for small values of D , the d -wave solution is the strongest one. Remarkably, we find that this d -wave instability purely follows from the momentum dependence of the screened Coulomb interaction, similarly to the Kohn-Luttinger mechanism [47, 48]. In particular, we find that the d -wave solution survives with approximately the same strength if we completely ignore the effect of the Goldstone modes. However, it disappears once we replace the polarization operator $\Pi(\mathbf{q})$ in Eq. (24) with its momentum independent value at $\mathbf{q} = 0$, $\Pi(0) = N(0)$. Therefore, we conclude that the effective attraction in the d -wave channel originates from the momentum dependence of the screening.

We also see from Fig. 6 that the p -wave solution increases rapidly with D and becomes comparable to the d -wave solution at $D \approx 25$ nm. For larger values of the gate distance, the p -wave solution becomes the dominant instability. We find that the attraction in the p -wave channel comes from the Goldstone-mediated interaction, while the Coulomb interaction tends to suppress it.

For small values of D , we also find a subleading instability in the s -wave channel, corresponding to s^{+-} pairing

with different signs of the superconducting gap on different Fermi surfaces. However, this instability quickly decreases as D increases and it never becomes competitive with either the d - or p -wave channel.

In the experiments of Ref. [40], the gate distance of the device displaying superconductivity around charge neutrality was approximately 12 nm, which according to Fig. 6 puts us in the regime where the d -wave channel is the strongest one, with $\lambda_d \approx 0.08$. Using the standard BCS analysis (see Appendix E), one obtains an estimate for the critical temperature given by

$$k_B T_c \sim \varepsilon_F \times e^{-1/\lambda}. \quad (40)$$

Using $\varepsilon_F = 3.2 \text{ meV}$ and $\lambda \approx 0.08$, one finds $T_c \approx 1.3 \times 10^{-4} \text{ K}$, which is too low compared to the experimental values of $T_c \approx 0.3 \text{ K}$. However, because of the exponential dependence of T_c on λ , we would obtain a value for the critical temperature which is comparable to the experimental values if λ_d was larger by a factor of only 2–2.5. There can be many reasons for why our simplified analysis is off by a factor of this magnitude. For example, we have not taken the mass renormalization of the electrons near the Fermi surface into account. Both the Coulomb and the Goldstone mode-mediated interaction will lead to a higher effective mass m^* , and therefore also to a higher density of states, resulting in enhanced values for λ in all channels.

VI. DISCUSSION

A. Comparison to other pairing mechanisms

Numerous other pairing mechanisms for superconductivity in tBLG have been discussed previously in the literature. In Refs. [3, 4, 6, 7, 13] it was proposed that tBLG is a conventional phonon-driven superconductor. References [2, 5, 8–10, 14–28, 46], on the other hand, have put forward a pairing mechanism which originates from the repulsive Coulomb or Hubbard interaction. There are several points which distinguish the results obtained in this paper from these previous works. First, our main focus is on doping regimes close to charge neutrality, while the majority of the previous works considered superconductivity near $\nu = \pm 2$. Secondly, many previous works which connect the superconducting domes in tBLG to a parent insulating state at integer filling start from an effective (Hubbard) model which is assumed to capture the same physics as the BM model. Here, on the other hand, we have used the actual BM Hamiltonian, keeping not only the flat bands but also some of the remote bands. And finally, many of the previous works which did use the BM model as a starting point considered Fermi surface instabilities of the “bare” nearly flat bands, while in this work we have studied Fermi surface instabilities of the self-consistent K-IVC bands. One advantage of

the latter approach is that the density of states in the K-IVC bands is much lower than the density of states of the original BM bands, which opens up the opportunity to meaningfully apply a weak-coupling approach.

Of all previous studies, Refs. [28] and [46] are most closely related to the present work. In particular, Ref. [28] also starts from the K-IVC insulator as the parent state for superconductivity, but it invokes a topological pairing mechanism, which is different from the weak-coupling superconducting instabilities discussed here. Additional study is required to better understand the interplay/competition between these two pairing mechanisms. Ref. [46] also considered valley Goldstone mode exchange as a mechanism for superconductivity in tBLG, but the inter-valley coherent insulator of Ref. [46] is different from the K-IVC insulator we consider in this work.

B. Outlook

To summarize, we have studied the potential connection between the insulating state observed in tBLG at charge neutrality [31, 38, 40] and the neighboring superconducting domes [31, 40]. Our starting point was to identify the insulating state with the K-IVC insulator of Ref. [42], which spontaneously breaks the valley- $U(1)$ symmetry. We have coupled the charge carriers at finite doping to the valley Goldstone modes and combined the resulting attractive interaction with the screened Coulomb interaction. We have then analysed the different weak-coupling superconducting instabilities resulting from the combined interaction. Depending on the distance between the tBLG device and the metallic gates, we found that the dominant pairing instability is either in the two-component d -wave or p -wave channel. Interestingly, pairing in the d -wave channel is generated by the Kohn-Luttinger-like mechanism via the momentum-dependent screening, while pairing in the p -wave channel is the result of Goldstone-mode exchange.

There is still a lot of room for improvement on the results presented here. Firstly, our starting point is a self-consistent Hartree-Fock band spectrum, and therefore ignores many-body correlation effects of the insulating state. Secondly, our analysis of the interactions that lead to the superconducting instabilities relies on the RPA approximation and thus ignores the effects of quantum fluctuations. Thirdly, our numerics were done on a 24×24 momentum grid, which introduces unknown finite-size errors in the numerical values for the different superconducting instabilities. And finally, the values for the critical temperature obtained via the standard BCS formula are too low compared to the experimental values [31, 40]. However, we hope that the approach put forward in this paper can be used as a starting point for future theoretical analytical and numerical works. For instance, a natural generalization of the present work would be to include the dynamical effects within the Eliashberg theory and investigate the role of the vertex corrections

to it, which were completely neglected in this study.

The present work also leaves several other questions unanswered, which deserve further theoretical investigation. For example, a better physical understanding of the numerically obtained net attractive interaction in the p -wave and d -wave channels is required. Also, it would be interesting to understand whether the same pairing mechanism for superconductivity could also be operative near $\nu = \pm 2$, as a spin polarized K-IVC state is expected to be a good candidate ground state at these even integer fillings [42]. In particular, if the same mechanism is at play near $\nu = \pm 2$, then it would be interesting to see whether the competing instabilities in the p -wave and d -wave channels could lead to nematic superconductivity, which was observed in Ref. [56] and discussed theoretically in Refs. [15–18].

The Hamiltonian of tBLG restricted to the nearly flat bands has an approximate $U(4) \times U(4)$ symmetry [42, 52], which is responsible for the close competition between many different symmetry-broken phases in self-consistent Hartree-Fock studies [34, 42, 57–59]. Because of this approximate symmetry, we expect the existence of many nearly soft bosonic modes corresponding to fluctuations within the low-energy $U(4) \times U(4)$ -manifold. In principle, all these modes can be important for superconductivity. One of these modes even becomes massless at the continuous phase transition between the K-IVC state and the valley-Hall state, which occurs when the microscopic sublattice splitting induced by the hexagonal boron nitride substrate is around 10 meV [42]. In Appendix F, we argue that non-Fermi liquid physics is expected at this critical point, but that deviations from Fermi liquid theory will only manifest themselves on very long distance and time scales. A very interesting topic for future work is to further study the role of these nearly soft or critical bosonic modes.

We also expect that the development of numerical methods such as DMRG [60], quantum Monte Carlo [53, 61], or the functional renormalization group [21, 62, 63] will be invaluable to shed further light on the above mentioned questions.

VII. ACKNOWLEDGMENTS

M. Z. and N. B. would like to thank Ashvin Vishwanath, Eslam Khalaf, Shubhayu Chatterjee, and Shang Liu for collaboration on related projects, which were vital for the results obtained in this work. We also want to thank Jonathan Ruhman, Ashvin Vishwanath, Eslam Khalaf, and Shubhayu Chatterjee for useful discussions and comments. V. K. was supported by the Quantum Materials program at LBNL, funded by the US Department of Energy under Contract No. DE-AC02-05CH11231. M. Z. was supported by the Director, Office of Science, Office of Basic Energy Sciences, Materials Sciences and Engineering Division of the U.S. Department of Energy under contract no. DE-AC02-05-CH11231 (van

Appendix A: Calculation of $K(\mathbf{q})$ and ρ_s at charge neutrality

In this Appendix, we demonstrate how to calculate function $K(\mathbf{q})$ and parameter ρ_s introduced in Eq. (5) at charge neutrality, i.e., at zero doping. We start by defining the operator which generates spatially dependent valley rotations

$$\hat{Q} = \frac{1}{2} \int d\mathbf{r} \phi(\mathbf{r}) f_{\mathbf{r}}^{\dagger} \tau_z f_{\mathbf{r}} \quad (\text{A1})$$

and write it in the band basis of the BM model to obtain

$$\hat{Q} = \frac{1}{2\sqrt{A}} \sum_{\mathbf{k}, \mathbf{q}} \phi_{\mathbf{q}} c_{\mathbf{k}+\mathbf{q}}^{\dagger} \Lambda_{\mathbf{q}}(\mathbf{k}) \tau_z c_{\mathbf{k}}, \quad (\text{A2})$$

where A is the area of the system and $\Lambda_{\mathbf{q}}(\mathbf{k})$ are the form factors defined in Eq. (11). Next, we choose a particular gauge for the K-IVC order parameter and define the following Hamiltonian:

$$H[\phi] = H_0 + e^{-i\hat{Q}} H_{\Delta} e^{i\hat{Q}}, \quad (\text{A3})$$

where, in accordance with the main text, H_0 is the valley symmetric part of the K-IVC Hamiltonian and H_{Δ} is the K-IVC order parameter, $H_{\Delta} = \sum_{\mathbf{k}} c_{\mathbf{k}}^{\dagger} \Delta(\mathbf{k}) c_{\mathbf{k}}$.

Using the Hamiltonian in Eq. (A3) we obtain the free energy $F[\phi]$ as

$$\mathcal{Z}[\phi(\mathbf{r})] = e^{-\beta F[\phi(\mathbf{r})]} = \text{Tr} \left(e^{-\beta H[\phi(\mathbf{r})]} \right), \quad (\text{A4})$$

where the trace is over fermionic degrees of freedom. We can now do an expansion of the free energy in ϕ and write

$$F[\phi(\mathbf{r})] = F_0 + \frac{1}{2} \int d^2\mathbf{r} \phi(\mathbf{r}) \hat{K} \phi(\mathbf{r}) + \dots, \quad (\text{A5})$$

where \hat{K} is a general differential operator. Going to momentum space, we obtain

$$F[\phi(\mathbf{q})] = F_0 + \frac{1}{2} \sum_{\mathbf{q}} \phi(\mathbf{q}) K(\mathbf{q}) \phi(-\mathbf{q}) + \dots, \quad (\text{A6})$$

In our discussion in the main text, we are interested in the function $K(\mathbf{q})$, which we can obtain as

$$K(\mathbf{q}) = \left. \frac{\delta^2 F[\phi]}{\delta \phi(\mathbf{q}) \delta \phi(-\mathbf{q})} \right|_{\phi=0} = -\frac{1}{\beta} \left. \frac{\delta^2 \ln \mathcal{Z}[\phi]}{\delta \phi(\mathbf{q}) \delta \phi(-\mathbf{q})} \right|_{\phi=0}. \quad (\text{A7})$$

To obtain a more convenient formula for $K(\mathbf{q})$ from Eq. (A7), we first expand the Hamiltonian to second order in ϕ , which gives

$$H[\phi] = H_0 + H_K - i[\hat{Q}, H_{\Delta}] - \frac{1}{2} [\hat{Q}, [\hat{Q}, H_{\Delta}]] + \dots \quad (\text{A8})$$

Writing this in the K-IVC band basis, we obtain

$$H[\phi] = \sum_{\mathbf{k}} \sum_{\alpha} E_{\alpha, \mathbf{k}} \psi_{\alpha, \mathbf{k}}^{\dagger} \psi_{\beta, \mathbf{k}} + \frac{1}{\sqrt{A}} \sum_{\mathbf{k}, \mathbf{q}} \sum_{\alpha, \beta} \phi(\mathbf{q}) g_{\alpha\beta}(\mathbf{k}, \mathbf{q}) \psi_{\alpha, \mathbf{k}+\mathbf{q}}^{\dagger} \psi_{\beta, \mathbf{k}}, \quad (\text{A9})$$

$$+ \frac{1}{2A} \sum_{\mathbf{k}, \mathbf{q}, \mathbf{q}'} \sum_{\alpha, \beta} \phi(\mathbf{q}) \phi(\mathbf{q}') \tilde{g}_{\alpha\beta}(\mathbf{k}, \mathbf{q}, \mathbf{q}') \psi_{\alpha, \mathbf{k}+\mathbf{q}+\mathbf{q}'}^{\dagger} \psi_{\beta, \mathbf{k}}, \quad (\text{A10})$$

where

$$g_{\alpha\beta}(\mathbf{k}, \mathbf{q}) = \frac{i}{2} \langle u_{\alpha, \mathbf{k}+\mathbf{q}} | (\Delta(\mathbf{k} + \mathbf{q}) \Lambda_{\mathbf{q}}(\mathbf{k}) \tau_z - \tau_z \Lambda_{\mathbf{q}}(\mathbf{k}) \Delta(\mathbf{k})) | u_{\beta, \mathbf{k}} \rangle \quad (\text{A11})$$

$$\begin{aligned} \tilde{g}_{\alpha\beta}(\mathbf{k}, \mathbf{q}, \mathbf{q}') = & -\frac{1}{4} \langle u_{\alpha, \mathbf{k}+\mathbf{q}+\mathbf{q}'} | \left(\Delta(\mathbf{k} + \mathbf{q} + \mathbf{q}') \Lambda_{\mathbf{q}}(\mathbf{k} + \mathbf{q}') \Lambda_{\mathbf{q}'}(\mathbf{k}) + \Lambda_{\mathbf{q}'}(\mathbf{k} + \mathbf{q}) \Delta(\mathbf{k} + \mathbf{q}) \Lambda_{\mathbf{q}}(\mathbf{k}) \right. \\ & \left. + \Lambda_{\mathbf{q}}(\mathbf{k} + \mathbf{q}') \Delta(\mathbf{k} + \mathbf{q}') \Lambda_{\mathbf{q}'}(\mathbf{k}) + \Lambda_{\mathbf{q}'}(\mathbf{k} + \mathbf{q}) \Lambda_{\mathbf{q}}(\mathbf{k}) \Delta(\mathbf{k}) \right) | u_{\beta, \mathbf{k}} \rangle, \end{aligned} \quad (\text{A12})$$

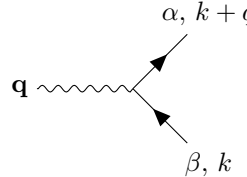
and $|u_{\alpha, \mathbf{k}}\rangle$ are the eigenstates of the K-IVC Hamiltonian. Next, we write the partition function as a path integral

$$\mathcal{Z}[\phi] = \int D\bar{\psi} D\psi e^{-S}, \quad (\text{A13})$$

where the imaginary-time action is given by

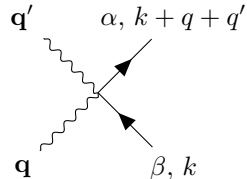
$$\begin{aligned} S = & \sum_{k=\mathbf{k}, i\omega_n} \bar{\psi}_{\alpha}(k) (-i\omega_n + E_{\mathbf{k}, \alpha}) \psi_{\alpha}(k) + \frac{1}{\sqrt{A}} \sum_{\mathbf{q}} \phi(\mathbf{q}) g_{\alpha\beta}(\mathbf{k}, \mathbf{q}) \bar{\psi}_{\alpha}(k + \mathbf{q}) \psi_{\beta}(k) \\ & + \frac{1}{2A} \sum_{\mathbf{q}, \mathbf{q}'} \phi(\mathbf{q}) \phi(\mathbf{q}') \tilde{g}_{\alpha\beta}(\mathbf{k}, \mathbf{q}, \mathbf{q}') \bar{\psi}_{\alpha}(k + \mathbf{q} + \mathbf{q}') \psi_{\beta}(k). \end{aligned} \quad (\text{A14})$$

This action contains the vertices



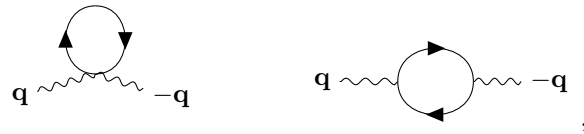
$$= ig_{\alpha\beta}(\mathbf{k}, \mathbf{q}) \quad (\text{A15})$$

and



$$= -\frac{1}{2} \tilde{g}_{\alpha\beta}(\mathbf{k}, \mathbf{q}, \mathbf{q}'). \quad (\text{A16})$$

Using Eq. (A7), one finds that $K(\mathbf{q})$ is given by the sum of the following two diagrams:



$$, \quad (\text{A17})$$

where the first diagram represents the diamagnetic contribution to the stiffness and the second diagram is the paramagnetic contribution.

The diamagnetic contribution is evaluated to give

$$K_{dia}(\mathbf{q}) = \frac{2}{A} \sum_{\mathbf{k}} \sum_{\alpha} f_{\alpha, \mathbf{k}} \tilde{g}_{\alpha\alpha}(\mathbf{k}, \mathbf{q}, -\mathbf{q}), \quad (\text{A18})$$

where $f_{\alpha, \mathbf{k}} = f(E_{\alpha, \mathbf{k}})$ is the Fermi-Dirac distribution function and the factor of two comes from the spin degeneracy. The paramagnetic contribution, on the other hand, equals

$$K_{para}(\mathbf{q}) = \frac{2}{A} \sum_{\mathbf{k}} \sum_{\alpha, \beta} \frac{f_{\beta, \mathbf{k}} - f_{\alpha, \mathbf{k}+\mathbf{q}}}{E_{\beta, \mathbf{k}} - E_{\alpha, \mathbf{k}+\mathbf{q}}} |g_{\alpha\beta}(\mathbf{k}, \mathbf{q})|^2. \quad (\text{A19})$$

Both $K_{dia}(\mathbf{q})$ and $K_{para}(\mathbf{q})$ are easily evaluated numerically from the mean-field K-IVC band structure, and $K(\mathbf{q})$ is then simply given by $K(\mathbf{q}) = K_{dia}(\mathbf{q}) + K_{para}(\mathbf{q})$. From $K(\mathbf{q})$, one obtains the K-IVC stiffness ρ_s by fitting (at zero temperature) the long wavelength part of $K(\mathbf{q}) = \rho_s \mathbf{q}^2 + \mathcal{O}(\mathbf{q}^4)$. Note that the zeroth order term in the long wavelength expansion of $K(\mathbf{q})$ has to vanish since the bosonic field ϕ describes massless Goldstone modes. In the next Appendix, we will explicitly show that this zeroth order (mass) term is indeed zero.

Appendix B: Calculation of χ_s at charge neutrality

To find χ_s in Eq. (5), we do a calculation analogous to what we did in the previous Appendix to obtain $K(\mathbf{q})$. The difference is that now we take ϕ to be spatially uniform but dependent on imaginary time. As before, we start by defining the free energy corresponding to the Hamiltonian (A3)

$$\mathcal{Z}[\phi(\tau)] = e^{-\beta F[\phi(\tau)]} = \text{tr} \left(e^{-\beta H[\phi(\tau)]} \right), \quad (\text{B1})$$

and expand it as

$$F[\phi(\tau)] = F_0 + \frac{1}{2\beta} \int_0^\beta d\tau \int d^2\mathbf{r} \chi_s (\partial_\tau \phi)^2 + \dots = F_0 + \frac{A}{2} \sum_{\nu_n} \phi(\nu_n) \chi_s \nu_n^2 \phi(-\nu_n) + \dots \quad (\text{B2})$$

From this expression we see that χ_s is given by

$$\chi_s = -\frac{1}{A\beta} \left(\frac{1}{\nu_n^2} \frac{\delta^2 \ln \mathcal{Z}}{\delta\phi(\nu_n) \delta\phi(-\nu_n)} \right) \Bigg|_{\nu_n=0, \phi=0}. \quad (\text{B3})$$

To obtain a more explicit formula for κ , we again expand $H[\phi(\tau)]$ in Eq. (A3) to the second order in $\phi(\tau)$:

$$\begin{aligned} H[\phi(\tau)] &= H_0 + H_\Delta - i[\hat{Q}, H_\Delta] - \frac{1}{2}[\hat{Q}, [\hat{Q}, H_\Delta]] + \dots \\ &= \sum_{\mathbf{k}} c_{\mathbf{k}}^\dagger \left(h_0(\mathbf{k}) + \Delta(\mathbf{k}) - \frac{i}{2} \phi(\tau) [\tau_z, \Delta(\mathbf{k})] - \phi^2(\tau) \frac{1}{8} [\tau_z, [\tau_z, \Delta(\mathbf{k})]] + \dots \right) c_{\mathbf{k}}, \end{aligned} \quad (\text{B4})$$

and write the partition function as a path integral where the action contains the vertices

$$\begin{array}{c} \beta, k+q \\ \nearrow \\ \nu_m \text{ wavy line} \\ \searrow \\ \alpha, k \end{array} = \frac{1}{2} [\tau_z, \Delta(\mathbf{k})]_{\alpha, \beta} \quad [q = (i\nu_m, 0)] \quad (\text{B5})$$

and

$$\begin{array}{c} \nu'_m \text{ wavy line} \\ \nearrow \\ \beta, k+q+q' \\ \searrow \\ \nu_m \text{ wavy line} \\ \searrow \\ \alpha, k \end{array} = \frac{1}{8} [\tau_z, [\tau_z, \Delta(\mathbf{k})]]_{\alpha, \beta} \quad [q = (i\nu_m, 0), q' = (i\nu'_m, 0)]. \quad (\text{B6})$$

The quantity $-(\beta A)^{-1} \delta^2 \ln \mathcal{Z} / (\delta\phi(\nu_m) \delta\phi(-\nu_m)) \Big|_{\phi=0}$ is given by two diagrams corresponding to a diamagnetic and paramagnetic contribution:

$$\begin{array}{c} \text{Diamagnetic diagram: } \nu_m \text{ wavy line} \rightarrow \text{circle with two arrows} \rightarrow -\nu_m \text{ wavy line} \\ \text{Paramagnetic diagram: } \nu_m \text{ wavy line} \rightarrow \text{circle with one arrow} \rightarrow -\nu_m \text{ wavy line} \end{array} \quad (\text{B7})$$

The diamagnetic contribution can be written as

$$\begin{aligned} & -\frac{1}{4\beta A} \sum_{\mathbf{k}} \sum_{\omega_n} \text{tr} \left([\tau_z, [\tau_z, \Delta(\mathbf{k})]] \frac{1}{i\omega_n - h_0(\mathbf{k}) - \Delta(\mathbf{k})} \right) \\ & = \frac{1}{4\beta A} \sum_{\mathbf{k}} \sum_{\omega_n} \text{tr} \left([\tau_z, \Delta(\mathbf{k})] \frac{1}{i\omega_n - h_0(\mathbf{k}) - \Delta(\mathbf{k})} [\tau_z, \Delta(\mathbf{k})] \frac{1}{i\omega_n - h_0(\mathbf{k}) - \Delta(\mathbf{k})} \right), \end{aligned} \quad (\text{B8})$$

To obtain the equality in the second line we have used the identities $\text{tr}([A, B]C) = -\text{tr}(B[A, C])$ and $[A, B^{-1}] = -B^{-1}[A, B]B^{-1}$, where A, B , and C are arbitrary matrices (and B is invertible for the second identity). We have also used the fact that $[\tau_z, h_0(\mathbf{k})] = 0$.

The paramagnetic contribution is given by

$$-\frac{1}{4\beta A} \sum_{\mathbf{k}} \sum_{\omega_n} \text{tr} \left([\tau_z, \Delta(\mathbf{k})] \frac{1}{i\omega_n + i\nu_n - h_0(\mathbf{k}) - \Delta(\mathbf{k})} [\tau_z, \Delta(\mathbf{k})] \frac{1}{i\omega_n - h_0(\mathbf{k}) - \Delta(\mathbf{k})} \right). \quad (\text{B9})$$

We see that for $\nu_n = 0$ the two diagrams exactly cancel each other, as it should be in the case of massless Goldstone modes. Let us now rewrite Eq. (B9) in the eigenbasis of the K-IVC Hamiltonian $h_0(\mathbf{k}) + \Delta(\mathbf{k})$. We find for the paramagnetic contribution

$$\begin{aligned} & -\frac{1}{2\beta A} \sum_{\mathbf{k}} \sum_{\omega_n} \sum_{\alpha, \beta} \langle u_{\alpha, \mathbf{k}} | [\tau_z, \Delta(\mathbf{k})] | u_{\beta, \mathbf{k}} \rangle \langle u_{\beta, \mathbf{k}} | [\tau_z, \Delta(\mathbf{k})] | u_{\alpha, \mathbf{k}} \rangle \frac{1}{i\omega_n + i\nu_n - E_{\alpha, \mathbf{k}}} \frac{1}{i\omega_n - E_{\beta, \mathbf{k}}} \\ & = \frac{1}{2A} \sum_{\mathbf{k}} \sum_{\alpha, \beta} \frac{f_{\beta, \mathbf{k}} - f_{\alpha, \mathbf{k}}}{i\nu_n + E_{\beta, \mathbf{k}} - E_{\alpha, \mathbf{k}}} |\langle u_{\alpha, \mathbf{k}} | [\tau_z, \Delta(\mathbf{k})] | u_{\beta, \mathbf{k}} \rangle|^2, \end{aligned} \quad (\text{B10})$$

where $|u_{\alpha, \mathbf{k}}\rangle$ are again the eigenstates of the K-IVC Hamiltonian and $E_{\alpha, \mathbf{k}}$ are the corresponding band energies. Expanding this term in $i\nu_n$ we find that the first order term vanishes, while the second order term gives us $\chi_s \nu_n^2$ (the zeroth order term is cancelled by the diamagnetic contribution). So we arrive at the following expression for χ_s :

$$\chi_s = -\frac{1}{2A} \sum_{\mathbf{k}} \sum_{\alpha, \beta} \frac{f_{\beta, \mathbf{k}} - f_{\alpha, \mathbf{k}}}{(E_{\beta, \mathbf{k}} - E_{\alpha, \mathbf{k}})^3} |\langle u_{\alpha, \mathbf{k}} | [\tau_z, \Delta(\mathbf{k})] | u_{\beta, \mathbf{k}} \rangle|^2. \quad (\text{B11})$$

This formula can be simplified by noting that $[\tau_z, \Delta(\mathbf{k})] = [\tau_z, h_0(\mathbf{k}) + \Delta(\mathbf{k})]$, which allows us to write

$$\chi_s = -\frac{1}{2A} \sum_{\mathbf{k}} \sum_{\alpha, \beta} \frac{f_{\beta, \mathbf{k}} - f_{\alpha, \mathbf{k}}}{E_{\beta, \mathbf{k}} - E_{\alpha, \mathbf{k}}} |\langle u_{\alpha, \mathbf{k}} | \tau_z | u_{\beta, \mathbf{k}} \rangle|^2. \quad (\text{B12})$$

So we find that, at zero temperature, χ_s is given by

$$\chi_s|_{T=0} = \frac{1}{A} \sum_{\mathbf{k}} \sum_{\alpha \in \text{occ}} \sum_{\beta \in \text{unocc}} \frac{|\langle u_{\alpha, \mathbf{k}} | \tau_z | u_{\beta, \mathbf{k}} \rangle|^2}{E_{\beta, \mathbf{k}} - E_{\alpha, \mathbf{k}}}. \quad (\text{B13})$$

Appendix C: Low-energy effective theory at non-zero doping

At non-zero doping, we can write down an effective low-energy theory to describe the electrons at the Fermi surface and the Goldstone modes. The total imaginary time action of this effective theory, obtained by integrating out the electrons in the K-IVC valence bands, is a sum of several terms:

$$S = S_\psi + S_C + S_{\psi-\phi} + S_{\psi-\phi^2} + S_\phi. \quad (\text{C1})$$

Below, we define and discuss each of these terms one by one.

The first term S_ψ is given by

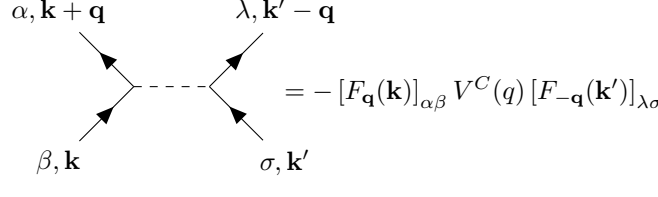
$$S_\psi = \int \frac{d\omega}{2\pi} \int_{\mathbf{k}} \bar{\psi}_\alpha(i\omega, \mathbf{k}) (-i\omega + E_{\alpha, \mathbf{k}}) \psi_\alpha(i\omega, \mathbf{k}) \quad (\text{C2})$$

and describes the electrons in the K-IVC conduction bands, meaning that $\alpha > 0$. Note that spin indices are always implicit, and that we have introduced the notation $\int_{\mathbf{k}} = \int \frac{d\mathbf{k}}{(2\pi)^2}$. We will represent propagators of the conduction band electrons diagrammatically in the conventional way, i.e., by a solid straight line with an arrow.

The second term S_C is the Coulomb interaction:

$$S_C = \frac{1}{2} \int_{\mathbf{q}} V_C(q) \rho_{\mathbf{q}} \rho_{-\mathbf{q}}, \quad (\text{C3})$$

where $V_C(q)$ is the gate-screened Coulomb potential defined in Eq. (19) and $\rho_{\mathbf{q}}$ is the density of electrons in the conduction bands as defined in Eq. (20). Diagrammatically, we will represent the Coulomb interaction between the electrons in the K-IVC conduction bands as

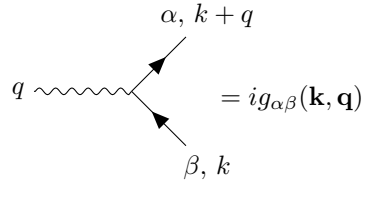


$$= -[F_{\mathbf{q}}(\mathbf{k})]_{\alpha\beta} V^C(q) [F_{-\mathbf{q}}(\mathbf{k}')]_{\lambda\sigma} \quad (\text{C4})$$

The third and fourth terms in Eq. (C1) describe the coupling between the electrons and the Goldstone boson field ϕ . In particular, the third term is given by

$$S_{\psi-\phi} = \int d\tau \int_{\mathbf{k}, \mathbf{q}} g_{\alpha\beta}(\mathbf{k}, \mathbf{q}) \phi(\tau, \mathbf{q}) \bar{\psi}_{\alpha}(\tau, \mathbf{k} + \mathbf{q}) \psi_{\beta}(\tau, \mathbf{k}), \quad (\text{C5})$$

where the coupling $g_{\alpha\beta}(\mathbf{k}, \mathbf{q})$ is defined in Eq. (16). As before, we represent the corresponding vertex diagrammatically as

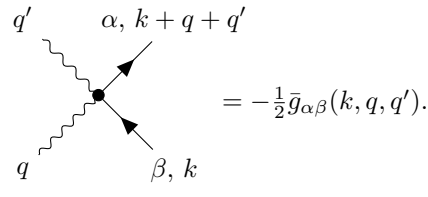


$$= i g_{\alpha\beta}(\mathbf{k}, \mathbf{q}). \quad (\text{C6})$$

The fourth term $S_{\psi-\phi^2}$ takes the form

$$S_{\psi-\phi^2} = \frac{1}{2} \int_{k, q, q'} \bar{g}_{\alpha\beta}(k, q, q') \phi(q) \phi(q') \bar{\psi}_{\alpha}(k + q + q') \psi_{\beta}(k), \quad (\text{C7})$$

where $k = (i\omega, \mathbf{k})$, $q = (i\nu, \mathbf{q})$, and $q' = (i\nu', \mathbf{q}')$ are three-vectors containing both frequency and momentum components, and $\int_k \equiv \int \frac{d\omega}{2\pi} \int_{\mathbf{k}}$. The corresponding vertex is represented diagrammatically as

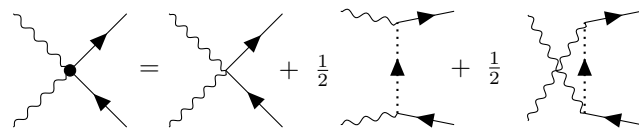


$$= -\frac{1}{2} \bar{g}_{\alpha\beta}(k, q, q'). \quad (\text{C8})$$

The coupling $\bar{g}_{\alpha\beta}(k, q, q')$ contains three different contributions. The first “bare” contribution comes from the second order term in the expansion of $e^{-i\hat{Q}} H_{\Delta} e^{i\hat{Q}}$, which, as discussed in Appendix A, leads to the coupling $\tilde{g}_{\alpha\beta}(\mathbf{k}, \mathbf{q}, \mathbf{q}')$ defined in Eq. (A12). For future convenience, we point out that this coupling satisfies

$$\tilde{g}_{\alpha\beta}(\mathbf{k}, 0, 0) = -\frac{1}{4} \langle u_{\alpha, \mathbf{k}} | [\tau_z, [\tau_z, \Delta(\mathbf{k})]] | u_{\beta, \mathbf{k}} \rangle. \quad (\text{C9})$$

The other two “renormalization” contributions to $\bar{g}_{\alpha\beta}(k, q, q')$ are the result of integrating out the valence electrons. The easiest way to represent these is to write out the different contributions to the coupling $\bar{g}_{\alpha\beta}(k, q, q')$ diagrammatically as follows:



$$= \text{bare vertex} + \frac{1}{2} \text{valence loop} + \frac{1}{2} \text{valence loop + Goldstone loop}, \quad (\text{C10})$$

where we have represented the propagator of the valence-band electrons by a dotted line with an arrow. The first diagram on the right hand side represents the “bare” coupling $\frac{1}{2} \tilde{g}_{\alpha\beta}(\mathbf{k}, \mathbf{q}, \mathbf{q}')$ discussed above. The last two diagrams

on the right hand side correspond to the “renormalization” contributions involving a virtual valence band electron, with two vertices given by $g_{\alpha\beta}(\mathbf{k}, \mathbf{q})$. Translating these diagrams into equations, the coupling $\bar{g}_{\alpha\beta}(k, q, q')$ is given by

$$\bar{g}_{\alpha\beta}(k, q, q') = \tilde{g}_{\alpha\beta}(\mathbf{k}, \mathbf{q}, \mathbf{q}') + \sum_{\gamma < 0} \left(\frac{g_{\alpha\gamma}(\mathbf{k} + \mathbf{q}, \mathbf{q}') g_{\gamma\beta}(\mathbf{k}, \mathbf{q})}{i(\omega + \nu) - E_{\lambda, \mathbf{k} + \mathbf{q}}} + \frac{g_{\alpha\gamma}(\mathbf{k} + \mathbf{q}', \mathbf{q}) g_{\gamma\beta}(\mathbf{k}, \mathbf{q}')}{i(\omega + \nu') - E_{\lambda, \mathbf{k} + \mathbf{q}'}} \right), \quad (\text{C11})$$

where the sum is over the K-IVC valence bands, labeled by negative integers.

The fourth term S_ϕ in Eq. (C1) is the “bare” quadratic boson action obtained after integrating out the valence electrons and expanding the free energy up to the second order in ϕ :

$$S_\phi = \frac{1}{2} \int \frac{d\omega}{2\pi} \int_{\mathbf{q}} \phi(i\omega, \mathbf{q}) K_0(\mathbf{q}) \phi(-i\omega, -\mathbf{q}), \quad (\text{C12})$$

where $K_0(\mathbf{q})$ is given by the diagram

$$K_0(\mathbf{q}) = \text{Diagram: a wavy line with a dashed loop on top, representing a bare boson propagator with a virtual valence band electron loop.} \quad (\text{C13})$$

which evaluates to

$$K_0(\mathbf{q}) = 2 \sum_{\alpha < 0} \int \frac{d\mathbf{k}}{(2\pi)^2} \tilde{g}_{\alpha\alpha}(\mathbf{k}, \mathbf{q}, -\mathbf{q}). \quad (\text{C14})$$

We would like to emphasize that the bare quantity $K_0(\mathbf{q})$ at finite doping is very different from the quantity $K(\mathbf{q})$ which we calculated in Appendix A at charge neutrality. In particular, in general $K_0(0)$ will not be equal to zero, such that the boson ϕ appears to be massive. To obtain a proper, massless Goldstone mode propagator, we need to “dress” it with the RPA self-energy, which contains two terms. The first term originates from the $\phi\bar{\psi}\psi$ coupling and is given by

$$\Sigma_G^p(i\omega, \mathbf{q}) = \text{Diagram: a wavy line with a solid loop on top, representing the first term of the RPA self-energy.} \quad (\text{C15})$$

The second contribution to the boson self-energy comes from the $\phi^2\bar{\psi}\psi$ coupling and is given by

$$\Sigma_G^d(i\omega, \mathbf{q}) = \text{Diagram: a wavy line with a solid loop on top and a dot on the wavy line, representing the second term of the RPA self-energy.} \quad (\text{C16})$$

Using the definition of the $\phi^2\bar{\psi}\psi$ coupling in Eq. (C10), we can rewrite this as

$$\text{Diagram: a wavy line with a solid loop on top and a dot on the wavy line} = \text{Diagram: a wavy line with a solid loop on top} + \text{Diagram: a wavy line with a dashed loop on top} + \text{Diagram: a wavy line with a dashed loop on top and a dot on the wavy line}. \quad (\text{C17})$$

Evaluating all diagrams we find that the boson self-energy is given by

$$\begin{aligned} \Sigma_G(i\omega, \mathbf{q}) &= \Sigma_G^p(i\omega, \mathbf{q}) + \Sigma_G^d(i\omega, \mathbf{q}) \\ &= 2 \sum_{\alpha, \beta} \int \frac{d\mathbf{k}}{(2\pi)^2} \frac{n_{\alpha, \mathbf{k} + \mathbf{q}} - n_{\beta, \mathbf{k}}}{i\omega + E_{\alpha, \mathbf{k} + \mathbf{q}} - E_{\beta, \mathbf{k}}} |g_{\alpha\beta}(\mathbf{k}, \mathbf{q})|^2 + 2 \sum_{\alpha > 0} \int \frac{d\mathbf{k}}{(2\pi)^2} n_{\alpha, \mathbf{k}} \tilde{g}_{\alpha\alpha}(\mathbf{k}, \mathbf{q}, -\mathbf{q}), \end{aligned} \quad (\text{C18})$$

where the factors of two again come from spin degeneracy, and the indices α and β in the first term run over both the K-IVC valence and conduction bands, i.e., α and β run over both positive and negative integers.

Including the self-energy, the “dressed” boson propagator equals

$$D_R^{-1}(i\omega, \mathbf{q}) = -K_0(\mathbf{q}) - \Sigma_G(i\omega, \mathbf{q}). \quad (\text{C19})$$

We now claim that the properly “dressed” propagator does describe a massless boson, and therefore satisfies the following equation:

$$K_0(0) + \Sigma_G(0, 0) = 0. \quad (\text{C20})$$

To show that this condition is indeed satisfied, we start with using Eq. (17) to write

$$\frac{n_{\alpha, \mathbf{k}} - n_{\beta, \mathbf{k}}}{E_{\alpha, \mathbf{k}} - E_{\beta, \mathbf{k}}} |g_{\alpha\beta}(\mathbf{k}, 0)|^2 = -\frac{1}{4} (n_{\alpha, \mathbf{k}} - n_{\beta, \mathbf{k}}) \langle u_{\alpha, \mathbf{k}} | [\tau_z, \Delta(\mathbf{k})] u_{\beta, \mathbf{k}} \rangle \langle u_{\beta, \mathbf{k}} | \tau_z | u_{\alpha, \mathbf{k}} \rangle. \quad (\text{C21})$$

Summing over both α and β in Eq. (C21), we obtain

$$\sum_{\alpha, \beta} \frac{n_{\alpha, \mathbf{k}} - n_{\beta, \mathbf{k}}}{E_{\alpha, \mathbf{k}} - E_{\beta, \mathbf{k}}} |g_{\alpha\beta}(\mathbf{k}, 0)|^2 = -\frac{1}{4} [\text{tr}(P_{\mathbf{k}}^o [\tau_z, \Delta(\mathbf{k})] P_{\mathbf{k}}^u \tau_z) - \text{tr}(P_{\mathbf{k}}^u [\tau_z, \Delta(\mathbf{k})] P_{\mathbf{k}}^o \tau_z)], \quad (\text{C22})$$

where $P_{\mathbf{k}}^o = \sum_{\alpha} n_{\alpha, \mathbf{k}} |u_{\alpha, \mathbf{k}} \rangle \langle u_{\alpha, \mathbf{k}}|$ is the projector onto the occupied states in the K-IVC bands at momentum \mathbf{k} , and $P_{\mathbf{k}}^u = \sum_{\alpha} (1 - n_{\alpha, \mathbf{k}}) |u_{\alpha, \mathbf{k}} \rangle \langle u_{\alpha, \mathbf{k}}|$ is the projector onto the unoccupied states at \mathbf{k} . Using $P_{\mathbf{k}}^u = \mathbf{1} - P_{\mathbf{k}}^o$, we find

$$\sum_{\alpha, \beta} \frac{n_{\alpha, \mathbf{k}} - n_{\beta, \mathbf{k}}}{E_{\alpha, \mathbf{k}} - E_{\beta, \mathbf{k}}} |g_{\alpha\beta}(\mathbf{k}, 0)|^2 = \frac{1}{4} \text{tr}(P_{\mathbf{k}}^o [\tau_z, [\tau_z, \Delta(\mathbf{k})]]) = -\sum_{\alpha} n_{\alpha, \mathbf{k}} \tilde{g}_{\alpha\alpha}(\mathbf{k}, 0, 0), \quad (\text{C23})$$

where for the last equality we have used Eq. (C9). Combining Eqs. (C23), (C18), and (C14), one finds that Eq. (C20) indeed holds, i.e., that $K_0(0) + \Sigma_G(0, 0) = 0$.

Since the bare boson propagator does not describe a massless Goldstone mode, it is crucial to always use the dressed propagator $D_R(i\omega, \mathbf{q})$ to investigate the effect of the Goldstone modes on the conductive electrons. For small enough doping, the “dressed” propagator $D_R(i\omega, \mathbf{q})$ will be very close to $D(i\omega, \mathbf{q})$, the propagator of the Goldstone modes at charge neutrality. This is because $D_R^{-1}(i\omega, \mathbf{q}) \approx \chi_R(\nu)(i\omega)^2 - \rho_R(\nu)\mathbf{q}^2$ changes continuously with doping and crosses over to $D^{-1}(i\omega, \mathbf{q}) \approx \chi_s(i\omega)^2 - \rho_s\mathbf{q}^2$ at $\nu = 0$. We have numerically verified that $D_R^{-1}(i\omega, \mathbf{q})$ at $\nu = 1/4$ is indeed close to $D^{-1}(i\omega, \mathbf{q})$. In the main text, we therefore use $D_R^{-1}(i\omega, \mathbf{q}) = D^{-1}(i\omega, \mathbf{q})$ for simplicity. The main motivation for this is that we found the propagator obtained at charge neutrality to be less prone to numerical error.

Using the propagator $D(i\omega, \mathbf{q})$, the Goldstone mode-mediated interaction between the electrons is obtained from the following tree-level diagram:

$$= -V_{\alpha\beta\lambda\sigma}^G(i\omega, \mathbf{q}, \mathbf{k}, \mathbf{k}'), \quad (\text{C24})$$

where

$$V_{\alpha\beta\lambda\sigma}^G(i\omega, \mathbf{q}, \mathbf{k}, \mathbf{k}') = g_{\alpha\beta}(\mathbf{k}, \mathbf{q}) D(i\omega, \mathbf{q}) g_{\lambda\sigma}(\mathbf{k}', -\mathbf{q}). \quad (\text{C25})$$

Equations (25) and (26) in the main text are then obtained by considering the static limit of V^G , i.e., setting $\omega = 0$.

As a final step in our RPA analysis of the effective low-energy theory, we show that one can neglect the screening of the $\phi\bar{\psi}\psi$ coupling by the Coulomb interaction. The latter is given by the following series of diagrams:

$$+ \dots \quad (\text{C26})$$

Summing up this series, we find that the screened electron-boson coupling is given by

$$\begin{aligned}
g(\mathbf{k}, \mathbf{q})_{scr} &= g(\mathbf{k}, \mathbf{q}) + 2F_{\mathbf{q}}(\mathbf{k}) \frac{V_C(q)}{\epsilon(\mathbf{q})} \sum_{\alpha, \beta} \int \frac{d\mathbf{k}'}{(2\pi)^2} \frac{n_{\alpha, \mathbf{k}'+\mathbf{q}} - n_{\beta, \mathbf{k}'}}{E_{\alpha, \mathbf{k}'+\mathbf{q}} - E_{\beta, \mathbf{k}'}} [F_{\mathbf{q}}(\mathbf{k}')]_{\alpha\beta}^* g_{\alpha\beta}(\mathbf{k}', \mathbf{q}) \\
&\equiv g(\mathbf{k}, \mathbf{q}) + F_{\mathbf{q}}(\mathbf{k}) \frac{V_C(q)}{\epsilon(\mathbf{q})} \langle F^* g \rangle(\mathbf{q}), \tag{C27}
\end{aligned}$$

where in the last line we have introduced the notation $\langle F^* g \rangle$ to denote the bubble diagram with a F and a g vertex.

From Eq. (C27) we see that the amount of screening of the electron-boson coupling is determined by $V_C(q) \langle F^* g \rangle(\mathbf{q}) / \epsilon(\mathbf{q})$. We find numerically that $V_C(q) \langle F^* g \rangle(\mathbf{q}) / \epsilon(\mathbf{q})$ is small for small momentum transfers, implying that the electron-boson coupling is only weakly screened by the Coulomb interaction at long wavelengths. In particular, we find that $V_C(q) \langle F^* g \rangle(\mathbf{q}) / \epsilon(\mathbf{q}) \lesssim 0.5$ meV for $|\mathbf{q}| < \pi/2L_M \approx 2k_{F,1}$, where $k_{F,1}$ is the average Fermi momentum of the outer Fermi surface. This implies that the correction from screening is smaller than the typical values of the bare coupling by a factor of 10 – 20. We therefore conclude that the Coulomb screening of the electron-boson vertex does not play an important role, and we will simply ignore it.

We would like to point out that the insignificance of the electron-boson vertex screening is a non-trivial result. For example, if the form factors $F_{\mathbf{q}}(\mathbf{k})$ and the dependence of the coupling on the incoming momenta were to be ignored, then one would find a screened coupling $g(\mathbf{q})_{scr} = g(\mathbf{q})/\epsilon(\mathbf{q})$. In this case, the electron-boson vertex would be almost completely suppressed and the electrons would be effectively decoupled from the Goldstone modes. So the momentum dependence of both $F_{\mathbf{q}}(\mathbf{k})$ and $g(\mathbf{k}, \mathbf{q})$ is crucial to protect the electron-boson coupling from Coulomb screening.

Appendix D: Interactions in the Cooper channel and Kramers time-reversal symmetry

The goal of this Appendix is to show that the Coulomb and Goldstone-mediated interactions in the Cooper channel can be written as

$$\begin{aligned}
\hat{V}_{\alpha\beta}^C(\mathbf{k}', \mathbf{k}) &\equiv \sum_{\mathbf{G}} \frac{e^2}{2\epsilon_0\epsilon} \frac{\tanh(D|\mathbf{k}' - \mathbf{k} + \mathbf{G}|)}{|\mathbf{k}' - \mathbf{k} + \mathbf{G}| + k_s(\mathbf{k}' - \mathbf{k} + \mathbf{G})} [F_{\mathbf{k}' - \mathbf{k} + \mathbf{G}}(\mathbf{k})]_{\alpha\beta} [F_{\mathbf{k} - \mathbf{k}' - \mathbf{G}}(-\mathbf{k})]_{\alpha\beta} \\
&= e^{i\varphi_{\alpha}(\mathbf{k}')} \left(\sum_{\mathbf{G}} \frac{e^2}{2\epsilon_0\epsilon} \frac{\tanh(D|\mathbf{k}' - \mathbf{k} + \mathbf{G}|)}{|\mathbf{k}' - \mathbf{k} + \mathbf{G}| + k_s(\mathbf{k}' - \mathbf{k} + \mathbf{G})} | [F_{\mathbf{k}' - \mathbf{k} + \mathbf{G}}(\mathbf{k})]_{\alpha\beta} |^2 \right) e^{-i\varphi_{\beta}(\mathbf{k})}, \tag{D1}
\end{aligned}$$

where the sum is over moiré reciprocal lattice vectors \mathbf{G} and $e^{i\varphi_{\alpha}(\mathbf{k}')}$, $e^{-i\varphi_{\beta}(\mathbf{k})}$ are gauge-dependent phase factors.

We start by recalling the definition of the K-IVC form factors $F_{\mathbf{q}}(\mathbf{k})$:

$$[F_{\mathbf{q}}(\mathbf{k})]_{\alpha\beta} = \langle u_{\alpha, \mathbf{k}+\mathbf{q}} | \Lambda_{\mathbf{q}}(\mathbf{k}) | u_{\beta, \mathbf{k}} \rangle, \tag{D2}$$

where $|u_{\alpha, \mathbf{k}}\rangle$ are the K-IVC eigenstates. Because of the spinless time-reversal symmetry $\mathcal{T} = \tau_x K$ of the BM model, we can without loss of generality use BM form factors which satisfy $\Lambda_{-\mathbf{q}}(-\mathbf{k}) = \tau_x \Lambda_{\mathbf{q}}^*(\mathbf{k}) \tau_x$ and $\tau_z \Lambda_{\mathbf{q}}(\mathbf{k}) \tau_z = \Lambda_{\mathbf{q}}(\mathbf{k})$. Using these properties, we find that

$$[F_{-\mathbf{q}}(-\mathbf{k})]_{\alpha\beta} = \langle u_{\alpha, -\mathbf{k}-\mathbf{q}} | i\tau_y \Lambda_{\mathbf{q}}^*(\mathbf{k}) i\tau_y^T | u_{\beta, -\mathbf{k}} \rangle \tag{D3}$$

Because of the \mathcal{T}' symmetry, with $\mathcal{T}' = \tau_z \mathcal{T} = i\tau_y K$, the K-IVC eigenstates satisfy

$$\mathcal{T}' | u_{\beta, \mathbf{k}} \rangle = e^{i\varphi_{\beta}(\mathbf{k})} | u_{\beta, -\mathbf{k}} \rangle \Rightarrow i\tau_y^T | u_{\beta, -\mathbf{k}} \rangle = e^{-i\varphi_{\beta}(\mathbf{k})} | u_{\beta, \mathbf{k}} \rangle^*, \tag{D4}$$

where $e^{i\varphi_{\beta}(\mathbf{k})}$ is a gauge-dependent phase factor. Since $|u_{\alpha, \mathbf{k}+\mathbf{G}}\rangle = |u_{\alpha, \mathbf{k}}\rangle$, it follows that $e^{i\varphi_{\alpha}(\mathbf{k}+\mathbf{G})} = e^{i\varphi_{\alpha}(\mathbf{k})}$. Using Eq. (D4), one finds that the K-IVC form factors satisfy

$$[F_{-\mathbf{q}}(-\mathbf{k})]_{\alpha\beta} = e^{i[\varphi_{\alpha}(\mathbf{k}+\mathbf{q}) - \varphi_{\beta}(\mathbf{k})]} \langle u_{\alpha, \mathbf{k}+\mathbf{q}} | \Lambda_{\mathbf{q}}(\mathbf{k}) | u_{\beta, \mathbf{k}} \rangle^* = e^{i[\varphi_{\beta}(\mathbf{k}) - \varphi_{\alpha}(\mathbf{k}+\mathbf{q})]} [F_{\mathbf{q}}(\mathbf{k})]_{\alpha\beta}^*, \tag{D5}$$

which in turn implies Eq. (D1).

We can also show that the Goldstone-mediated interaction similarly satisfies

$$\begin{aligned}
\hat{V}_{\alpha\beta}^G(\mathbf{k}, \mathbf{k}') &\equiv - \sum_{\mathbf{G}} K(\mathbf{k}' - \mathbf{k} + \mathbf{G})^{-1} g_{\alpha\beta}(\mathbf{k}, \mathbf{k}' - \mathbf{k} + \mathbf{G}) g_{\alpha\beta}(-\mathbf{k}, \mathbf{k} - \mathbf{k}' - \mathbf{G}) \\
&= -e^{i\varphi_{\alpha}(\mathbf{k}')} \left(\sum_{\mathbf{G}} K(\mathbf{k}' - \mathbf{k} + \mathbf{G})^{-1} |g_{\alpha\beta}(\mathbf{k}, \mathbf{k}' - \mathbf{k} + \mathbf{G})|^2 \right) e^{-i\varphi_{\beta}(\mathbf{k})}. \tag{D6}
\end{aligned}$$

First, we again use the properties of the BM form factors and find

$$g_{\alpha\beta}(-\mathbf{k}, -\mathbf{q}) = \frac{i}{2} \langle u_{\alpha, -\mathbf{k}-\mathbf{q}} | \Delta(-\mathbf{k} - \mathbf{q}) i\tau_y \Lambda_{\mathbf{q}}^*(\mathbf{k}) i\tau_y^T \tau_z - \tau_z i\tau_y \Lambda_{\mathbf{q}}^*(\mathbf{k}) i\tau_y^T \Delta(-\mathbf{k}) | u_{\beta, -\mathbf{k}} \rangle. \quad (\text{D7})$$

The Kramers time-reversal symmetry of the K-IVC state implies that $i\tau_y^T \Delta(-\mathbf{k}) i\tau_y = \Delta^*(\mathbf{k})$, which allows us to write

$$g_{\alpha\beta}(-\mathbf{k}, -\mathbf{q}) = -\frac{i}{2} \langle u_{\alpha, -\mathbf{k}-\mathbf{q}} | i\tau_y [\Delta^*(\mathbf{k} + \mathbf{q}) \Lambda_{\mathbf{q}}^*(\mathbf{k}) \tau_z - \tau_z \Lambda_{\mathbf{q}}^*(\mathbf{k}) \Delta^*(\mathbf{k})] i\tau_y^T | u_{\beta, -\mathbf{k}} \rangle. \quad (\text{D8})$$

From the transformation property of the K-IVC states in Eq. (D4), we find that

$$g_{\alpha\beta}(-\mathbf{k}, -\mathbf{q}) = e^{i[\varphi_{\alpha}(\mathbf{k}+\mathbf{q}) - \varphi_{\beta}(\mathbf{k})]} g_{\alpha\beta}^*(\mathbf{k}, \mathbf{q}), \quad (\text{D9})$$

which implies Eq. (D6).

Appendix E: BCS gap equation

In the main text, we look for superconducting states with an order parameter of the form

$$\tilde{\Delta}_{\mathbf{k}}^s = \begin{pmatrix} \tilde{\Delta}_{1,\mathbf{k}} & 0 \\ 0 & \tilde{\Delta}_{2,\mathbf{k}} \end{pmatrix} \otimes i s_y, \quad (\text{E1})$$

$$\tilde{\Delta}_{\mathbf{k}}^t = \begin{pmatrix} \tilde{\Delta}_{1,\mathbf{k}} & 0 \\ 0 & \tilde{\Delta}_{2,\mathbf{k}} \end{pmatrix} \otimes i s_y \mathbf{s}, \quad (\text{E2})$$

which corresponds to a spin-singlet or spin-triplet pairing of electrons within the same band. The finite temperature gap equation is then given by

$$\tilde{\Delta}_{\alpha,\mathbf{k}} = -\frac{1}{A} \sum_{\beta,\mathbf{k}'} V_{\alpha\beta}(\mathbf{k}, \mathbf{k}') \frac{\tilde{\Delta}_{\beta,\mathbf{k}'}}{2\sqrt{E_{\beta,\mathbf{k}'}^2 + |\tilde{\Delta}_{\beta,\mathbf{k}'}|^2}} \tanh\left(\frac{\sqrt{E_{\beta,\mathbf{k}'}^2 + |\tilde{\Delta}_{\beta,\mathbf{k}'}|^2}}{2k_B T}\right), \quad (\text{E3})$$

where A is the area of the system. To find the critical temperature of possible superconducting states, we take the BCS gap equation and apply the standard procedure by ignoring the dependence on the gap in the denominator and the argument of the hyperbolic tangent in Eq. (E3), motivated by the fact that the gap goes to zero if we approach the critical temperature from below. This leaves us with

$$\begin{aligned} \tilde{\Delta}_{\alpha,\mathbf{k}} &= -\frac{1}{A} \sum_{\beta,\mathbf{k}'} V_{\alpha\beta}(\mathbf{k}, \mathbf{k}') \frac{\tilde{\Delta}_{\beta,\mathbf{k}'}}{2E_{\beta,\mathbf{k}'}} \tanh\left(\frac{E_{\beta,\mathbf{k}'}}{2k_B T_c}\right) \\ &\approx -\sum_{\beta} \int dE N_{\beta}(E) \int \frac{d\theta'}{2\pi} V_{\alpha\beta}[\mathbf{k}, \mathbf{k}'(E, \theta')] \frac{\tilde{\Delta}_{\beta,\mathbf{k}'(E, \theta')}}{2E} \tanh\left(\frac{E}{2k_B T_c}\right), \end{aligned} \quad (\text{E4})$$

where θ' is a polar angle in momentum space and

$$N_{\beta}(E) = \int \frac{d\theta}{2\pi} \frac{k_{\beta}(E, \theta)}{2\pi} \left| \frac{\partial E_{\beta}(k, \theta)}{\partial k} \right|_{k=k_{\beta}(E, \theta)}^{-1} \quad (\text{E5})$$

corresponds to the density of states in band β . Here, we use $k_{\beta}(E, \theta)$ to denote the inverse function of the dispersion $E_{\beta}(k, \theta)$, i.e., it is defined via the relation $E_{\beta}[k_{\beta}(E', \theta), \theta] = E'$. Note that the approximation in Eq. (E4) is justified if the dispersion near the Fermi surfaces is close to being isotropic.

Next, focusing on the vicinity of the Fermi surface, we write

$$\begin{aligned} \tilde{\Delta}_{\alpha,\mathbf{k}} &\approx -\sum_{\beta} N_{\beta}(0) \int \frac{d\theta'}{2\pi} V_{\alpha\beta}[\mathbf{k}, \mathbf{k}_{F,\beta}(\theta')] \tilde{\Delta}_{\beta,\mathbf{k}_{F,\beta}(\theta')} \int dE \frac{\tanh\left(\frac{E}{2k_B T_c}\right)}{2E} \\ &\Rightarrow \tilde{\Delta}_{\alpha}(\theta) \approx -\sum_{\beta} N_{\beta}(0) \int \frac{d\theta'}{2\pi} V_{\alpha\beta}(\theta, \theta') \tilde{\Delta}_{\beta}(\theta') \int dE \frac{\tanh\left(\frac{E}{2k_B T_c}\right)}{2E}, \end{aligned} \quad (\text{E6})$$

where $\mathbf{k}_{F,\beta}(\theta')$ is the angle-dependent Fermi momentum on the Fermi surface in band β . In the last line, we have introduced the notation $\Delta_\beta(\theta) = \Delta_{\beta,\mathbf{k}_{F,\alpha}(\theta)}$ for the gaps on the Fermi surfaces, and also $V_{\alpha\beta}(\theta, \theta') = V_{\alpha\beta}[\mathbf{k}_{F,\alpha}(\theta), \mathbf{k}_{F,\beta}(\theta')]$ for the interaction on the Fermi surfaces. $N_\beta(0)$ is the density of states of band β at the Fermi surface.

It is now clear that to find solutions of the gap equation, we have to solve the eigenvalue equation

$$\sum_\beta \int \frac{d\theta'}{2\pi} V_{\alpha\beta}(\theta, \theta') N_\beta(0) \tilde{\Delta}_\beta(\theta') = -\lambda \tilde{\Delta}_\alpha(\theta), \quad (\text{E7})$$

after which we can proceed with the solution of the gap equation in the standard way to obtain

$$k_B T_c \sim \varepsilon_F \times e^{-1/\lambda}, \quad (\text{E8})$$

where ε_F is the Fermi energy.

Appendix F: Continuous transition between K-IVC and valley Hall insulator

If the hexagonal boron-nitride (hBN) substrate encapsulating the tBLG system becomes sufficiently aligned with one of the graphene layers, it can introduce a significant C_{2z} -breaking sublattice splitting $\Delta_t \sigma_z$ via the proximity effect [64–67]. Here, σ_i are the Pauli matrices acting on the sublattice index. The sublattice splitting generates a Dirac mass at both the K and K' points of the mini-BZ, leading to an insulating single-particle spectrum at charge neutrality. Depending on the sign of the sublattice splitting, the spin resolved bands in each valley have Chern number ± 1 [68–70]. Note that time-reversal symmetry is not broken and that the bands in different valleys which are exchanged under time-reversal have opposite Chern numbers. Because only the valley-resolved Chern number of the filled bands is non-zero, this state is referred to as the valley Hall (VH) insulator.

In Ref. [42] it was found that within mean-field theory, there is a transition from the K-IVC insulator to the VH insulator at a critical sublattice splitting (say, on the top layer) of $\Delta_t^* \sim 10$ meV. At this point, there is a second order phase transition where both the $U_V(1)$ and time-reversal symmetry are restored. Importantly, the single-particle gap does not close at the transition. We also find that the Fermi surfaces around Γ at $\nu = 1/4$ do not change in any significant way if we tune through the transition. However, if Δ_t becomes sufficiently close to the critical value Δ_t^* , there is an additional soft (critical) bosonic mode which can facilitate pairing.

Based on experience with other systems with a Fermi surface coupled to a critical mode one naturally expects non-Fermi liquid behavior near the K-IVC – VH transition, even at small coupling [71–78]. We will argue that this expectation is essentially correct, but also that the non-Fermi liquid physics follows from very small, seemingly negligible terms. To set up the argument, let us actually start from the VH side, i.e., let us consider the system with $\Delta_t > \Delta_t^*$. Also, in this Appendix, we will work in the sublattice polarized basis introduced in Ref. [42]. As the precise definition of this basis is not relevant for this work, we will not give it here and just refer to Ref. [42] for details. The only reason why we use the sublattice polarized basis is that the K-IVC order parameter takes on a particularly simple form. Namely, in this basis we have $\Delta(\mathbf{k}) = [d_x(\mathbf{k})\tau_x + d_y(\mathbf{k})\tau_y]\sigma_y$, where τ_i are still the Pauli matrices acting on the valley index. The Yukawa coupling to the K-IVC modes which become soft near the critical point is then given by

$$H_Y = \frac{g}{N} \sum_{\mathbf{k}, \mathbf{q}} \tilde{c}_{\mathbf{k}+\mathbf{q}}^\dagger(\mathbf{q}\cdot)\sigma_y \tilde{c}_{\mathbf{k}}, \quad (\text{F1})$$

where $\mathbf{q}\cdot = \phi_{\mathbf{q}}^x \tau_x + \phi_{\mathbf{q}}^y \tau_y$. So the doped VH state coupled to the K-IVC modes is described by

$$H = \sum_{\mathbf{k}, \tau, \alpha} \varepsilon_{\tau, \alpha, \mathbf{k}} \tilde{c}_{\tau, \alpha, \mathbf{k}}^\dagger \tilde{c}_{\tau, \alpha, \mathbf{k}} + \frac{1}{N} \sum_{\mathbf{k}, \mathbf{q}} \sum_{\tau, \tau', \alpha, \beta} \langle w_{\tau, \alpha, \mathbf{k}+\mathbf{q}} | (\mathbf{q}\cdot)\sigma_y | w_{\tau', \beta, \mathbf{k}} \rangle \tilde{c}_{\tau, \alpha, \mathbf{k}+\mathbf{q}}^\dagger \tilde{c}_{\tau', \beta, \mathbf{k}}, \quad (\text{F2})$$

where $\varepsilon_{\tau, \alpha, \mathbf{k}}$ and $|w_{\tau, \alpha, \mathbf{k}}\rangle$ are the band energies and Bloch states of the mean-field VH Hamiltonian. Because the VH state preserves the valley symmetry, the eigenstates have a well-defined valley quantum number τ . The index α distinguishes between valence and conduction bands. Since we are interested in, e.g., electron doping, we neglect the valence bands and focus only on the conduction bands. This means that we can ignore the α index, and label the electrons by the valley index (and spin). We can then write the Hamiltonian as

$$H = \sum_{\mathbf{k}, \tau} \varepsilon_{\tau, \mathbf{k}} \tilde{c}_{\tau, \mathbf{k}}^\dagger \tilde{c}_{\tau, \mathbf{k}} + \frac{1}{N} \sum_{\mathbf{k}, \mathbf{q}} \left(g_{+-}(\mathbf{k}, \mathbf{q}) \phi_{\mathbf{q}}^+ \tilde{c}_{+, \mathbf{k}+\mathbf{q}}^\dagger \tilde{c}_{-, \mathbf{k}} + H.c. \right), \quad (\text{F3})$$

where in the last line we have introduced the notation $\phi_{\mathbf{q}}^+ = \phi_{\mathbf{q}}^x + i\phi_{\mathbf{q}}^y$ and

$$g_{+-}(\mathbf{k}, \mathbf{q}) = g \langle w_{+, \mathbf{k}+\mathbf{q}} | \tau_x \sigma_y | w_{-, \mathbf{k}} \rangle. \quad (\text{F4})$$

For our purposes, the main question we want to address is whether the coupling $g_{+-}(\mathbf{k}, \mathbf{q})$ becomes zero at zero momentum transfer, i.e., whether $g_{+-}(\mathbf{k}, 0) = 0$ or not.

Before we answer the above question, we first recall that the BM model has an emergent approximate particle-hole symmetry \mathcal{P} [79, 80], which acts in the sublattice polarized basis as [42]

$$\mathcal{P} : \tilde{c}_{\mathbf{k}}^\dagger \rightarrow \tau_z \sigma_y \tilde{c}_{-\mathbf{k}}. \quad (\text{F5})$$

If we combine the particle-hole symmetry with the time-reversal symmetry \mathcal{T} defined in Eq. (3), we obtain an approximate \mathcal{PT} symmetry acting as

$$\mathcal{PT} : \tilde{c}_{\mathbf{k}}^\dagger \rightarrow i\tau_y \sigma_y \tilde{c}_{\mathbf{k}}, \quad i \rightarrow -i. \quad (\text{F6})$$

Because of this approximate \mathcal{PT} symmetry we conclude that the dominant, particle-hole symmetric terms in the VH Hamiltonian anti-commute with $\tau_y \sigma_y$, and therefore also with $\tau_x \sigma_y$. But these matrices exactly constitute the K-IVC order parameter in the sublattice polarized basis. This implies that if the VH Hamiltonian was perfectly particle-hole symmetric, then the coupling would vanish for zero momentum transfer: $g_{+-}(\mathbf{k}, 0) = 0$. This is because $\tau_x \sigma_y$ anti-commutes with the particle-hole symmetric VH Hamiltonian, such that it maps a conduction band Bloch state to a valence band Bloch state and vice versa. Because of this, the matrix element in Eq. (F4) is strictly zero. Note that the full Yukawa coupling term in Eq. (F1) is not zero when $\mathbf{q} = 0$, only the part projected onto the conduction bands is. In other words, at $\mathbf{q} = 0$, the Yukawa coupling only mixes the valence and conduction bands of the particle-hole symmetric VH insulator, but it does not mix conduction bands among themselves. In part, this is a manifestation of the fact that the hBN sublattice splitting σ_z and the K-IVC order parameter $\tau_x \sigma_y$ anti-commute, which also implies that the electron gap at $\nu = 0$ does not close at the critical point.

In general, we of course have to include the small particle-hole symmetry breaking terms in the VH Hamiltonian. These terms give rise to a non-zero, but very small value for $g_{+-}(\mathbf{k}, 0)$.

Similar to the analysis in Ref. [81], we can now consider the electron interaction induced by the soft K-IVC modes for $\Delta_t \gtrsim \Delta_t^*$. It is given by [81]

$$V_{IVC}(\mathbf{k}, \mathbf{q}, \omega) = -|g_{+-}(\mathbf{k}, \mathbf{q})|^2 \chi(\mathbf{q}, \omega). \quad (\text{F7})$$

Here, $\chi(\mathbf{q}, \omega)$ is the valley- $U(1)$ susceptibility

$$\chi(\mathbf{q}, \omega) \sim \chi_0 \left(\frac{\xi^{-2}}{c^2 q^2 + \omega^2 + \xi^{-2}} \right)^{1-\eta/2}, \quad (\text{F8})$$

where $\xi \sim |\Delta_t - \Delta_t^*|^{-\nu} = |\delta\Delta_t|^{-\nu}$ is the correlation length of the boson field ϕ and $\chi_0 \sim |\delta\Delta_t|^{-\gamma}$. The critical exponents ν, γ , and η are those of the (2+1)- d $O(2)$ Wilson-Fisher fixed point [82].

Because g_{+-} is non-zero at $\mathbf{q} = 0$, the interaction $V_{IVC}(\mathbf{k}, 0, 0)$ in Eq. (F7) diverges at the critical point, resulting in non-Fermi liquid physics. However, because $g_{+-}(\mathbf{k}, 0)$ is very small, we only expect the non-Fermi liquid physics to manifest itself at very long distance and time scales.

-
- [1] Yuan Cao, Valla Fatemi, Shiang Fang, Kenji Watanabe, Takashi Taniguchi, Efthimios Kaxiras, and Pablo Jarillo-Herrero, “Unconventional superconductivity in magic-angle graphene superlattices,” *Nature* **556**, 43 (2018).
 - [2] Francisco Guinea and Niels R. Walet, “Electrostatic effects, band distortions, and superconductivity in twisted graphene bilayers,” *Proceedings of the National Academy of Sciences* **115**, 13174–13179 (2018).
 - [3] Fengcheng Wu, A. H. MacDonald, and Ivar Martin, “Theory of phonon-mediated superconductivity in twisted bilayer graphene,” *Phys. Rev. Lett.* **121**, 257001 (2018).
 - [4] Biao Lian, Zhijun Wang, and B. Andrei Bernevig, “Twisted bilayer graphene: A phonon-driven superconductor,” *Phys. Rev. Lett.* **122**, 257002 (2019).
 - [5] Yi-Zhuang You and Ashvin Vishwanath, “Superconductivity from valley fluctuations and approximate $SO(4)$ symmetry in a weak coupling theory of twisted bilayer graphene,” *npj Quantum Materials* **4**, 16 (2019).
 - [6] Teemu J. Peltonen, Risto Ojajarvi, and Tero T. Heikkila,

- “Mean-field theory for superconductivity in twisted bilayer graphene,” *Phys. Rev. B* **98**, 220504 (2018).
- [7] Young Woo Choi and Hyoung Joon Choi, “Strong electron-phonon coupling, electron-hole asymmetry, and nonadiabaticity in magic-angle twisted bilayer graphene,” *Phys. Rev. B* **98**, 241412 (2018).
- [8] Cenke Xu and Leon Balents, “Topological superconductivity in twisted multilayer graphene,” *Phys. Rev. Lett.* **121**, 087001 (2018).
- [9] Bitan Roy and Vladimir Juricic, “Unconventional superconductivity in nearly flat bands in twisted bilayer graphene,” *Phys. Rev. B* **99**, 121407 (2019).
- [10] Hiroki Isobe, Noah F. Q. Yuan, and Liang Fu, “Unconventional superconductivity and density waves in twisted bilayer graphene,” *Phys. Rev. X* **8**, 041041 (2018).
- [11] Yu-Ping Lin and Rahul M. Nandkishore, “Kohn-Luttinger superconductivity on two orbital honeycomb lattice,” *Phys. Rev. B* **98**, 214521 (2018).
- [12] Yu-Ping Lin and Rahul M. Nandkishore, “Chiral twist on the high- T_c phase diagram in moire heterostructures,” *Phys. Rev. B* **100**, 085136 (2019).
- [13] Fengcheng Wu, Euyheon Hwang, and Sankar Das Sarma, “Phonon-induced giant linear-in- T resistivity in magic angle twisted bilayer graphene: Ordinary strangeness and exotic superconductivity,” *Phys. Rev. B* **99**, 165112 (2019).
- [14] Girish Sharma, Maxim Trushin, Oleg P. Sushkov, Giovanni Vignale, and Shaffique Adam, “Superconductivity from collective excitations in magic angle twisted bilayer graphene,” arXiv eprints (2019), [arXiv:1909.02574](https://arxiv.org/abs/1909.02574) [cond-mat.mes-hall].
- [15] Vladyslav Kozii, Hiroki Isobe, Jörn W. F. Venderbos, and Liang Fu, “Nematic superconductivity stabilized by density wave fluctuations: Possible application to twisted bilayer graphene,” *Phys. Rev. B* **99**, 144507 (2019).
- [16] Dmitry V. Chichinadze, Laura Classen, and Andrey V. Chubukov, “Nematic superconductivity in twisted bilayer graphene,” arXiv e-prints (2019), [arXiv:1910.07379](https://arxiv.org/abs/1910.07379) [cond-mat.supr-con].
- [17] J. F. Dodaro, S. A. Kivelson, Y. Schattner, X. Q. Sun, and C. Wang, “Phases of a phenomenological model of twisted bilayer graphene,” *Phys. Rev. B* **98**, 075154 (2018).
- [18] Jörn W. F. Venderbos and Rafael M. Fernandes, “Correlations and electronic order in a two-orbital honeycomb lattice model for twisted bilayer graphene,” *Phys. Rev. B* **98**, 245103 (2018).
- [19] Sujay Ray, Jeil Jung, and Tanmoy Das, “Wannier pairs in superconducting twisted bilayer graphene and related systems,” *Phys. Rev. B* **99**, 134515 (2019).
- [20] Louk Rademaker and Paula Mellado, “Charge-transfer insulation in twisted bilayer graphene,” *Phys. Rev. B* **98**, 235158 (2018).
- [21] Dante M. Kennes, Johannes Lischner, and Christoph Karrasch, “Strong correlations and $d+id$ superconductivity in twisted bilayer graphene,” *Phys. Rev. B* **98**, 241407 (2018).
- [22] Cheng-Cheng Liu, Li-Da Zhang, Wei-Qiang Chen, and Fan Yang, “Chiral spin density wave and $d+id$ superconductivity in the magic-angle-twisted bilayer graphene,” *Phys. Rev. Lett.* **121**, 217001 (2018).
- [23] Huaiming Guo, Xingchuan Zhu, Shiping Feng, and Richard T. Scalettar, “Pairing symmetry of interacting fermions on a twisted bilayer graphene superlattice,” *Phys. Rev. B* **97**, 235453 (2018).
- [24] M. Fidrysiak, M. Zegrodnik, and J. Spalek, “Unconventional topological superconductivity and phase diagram for an effective two-orbital model as applied to twisted bilayer graphene,” *Phys. Rev. B* **98**, 085436 (2018).
- [25] J. Gonzalez and T. Stauber, “Kohn-Luttinger superconductivity in twisted bilayer graphene,” *Phys. Rev. Lett.* **122**, 026801 (2019).
- [26] Fengcheng Wu, “Topological chiral superconductivity with spontaneous vortices and supercurrent in twisted bilayer graphene,” *Phys. Rev. B* **99**, 195114 (2019).
- [27] Yury Sherkunov and Joseph J. Betouras, “Electronic phases in twisted bilayer graphene at magic angles as a result of Van Hove singularities and interactions,” *Phys. Rev. B* **98**, 205151 (2018).
- [28] Eslam Khalaf, Shubhayu Chatterjee, Nick Bultinck, Michael P. Zaletel, and Ashvin Vishwanath, “Charged Skyrmions and Topological Origin of Superconductivity in Magic Angle Graphene,” , arXiv:2004.00638 (2020), [arXiv:2004.00638](https://arxiv.org/abs/2004.00638) [cond-mat.str-el].
- [29] Yuan Cao, Valla Fatemi, Ahmet Demir, Shiang Fang, Spencer L Tomarken, Jason Y Luo, Javier D Sanchez-Yamagishi, Kenji Watanabe, Takashi Taniguchi, Efthimios Kaxiras, Ray C. Ashoori, and Pablo Jarillo-Herrero, “Correlated insulator behaviour at half-filling in magic-angle graphene superlattices,” *Nature* **556**, 80 (2018).
- [30] Matthew Yankowitz, Shaowen Chen, Hryhoriy Polshyn, Yuxuan Zhang, K. Watanabe, T. Taniguchi, David Graf, Andrea F. Young, and Cory R. Dean, “Tuning superconductivity in twisted bilayer graphene,” *Science* **363**, 1059–1064 (2019).
- [31] Xiaobo Lu, Petr Stepanov, Wei Yang, Ming Xie, Mohammed Ali Aamir, Ipsita Das, Carles Urgell, Kenji Watanabe, Takashi Taniguchi, Guangyu Zhang, Adrian Bachtold, Allan H. MacDonald, and Dmitri K. Efetov, “Superconductors, orbital magnets, and correlated states in magic angle bilayer graphene,” *Nature* **574**, 653–657 (2019).
- [32] Aaron L. Sharpe, Eli J. Fox, Arthur W. Barnard, Joe Finney, Kenji Watanabe, Takashi Taniguchi, M. A. Kastner, and David Goldhaber-Gordon, “Emergent ferromagnetism near three-quarters filling in twisted bilayer graphene,” *Science* **365**, 605–608 (2019).
- [33] M. Serlin, C. L. Tschirhart, H. Polshyn, Y. Zhang, J. Zhu, K. Watanabe, T. Taniguchi, L. Balents, and A. F. Young, “Intrinsic quantized anomalous hall effect in a moire heterostructure,” *Science* **367**, 900–903 (2020).
- [34] Youngjoon Choi, Jeannette Kemmer, Yang Peng, Alex Thomson, Harpreet Arora, Robert Polski, Yiran Zhang, Hechen Ren, Jason Alicea, Gil Refael, Felix von Oppen, Kenji Watanabe, Takashi Taniguchi, and Stevan Nadj-Perge, “Electronic correlations in twisted bilayer graphene near the magic angle,” *Nature Physics* (2019), [10.1038/s41567-019-0606-5](https://doi.org/10.1038/s41567-019-0606-5).
- [35] Alexander Kerelsky, Leo J. McGilly, Dante M. Kennes, Lede Xian, Matthew Yankowitz, Shaowen Chen, K. Watanabe, T. Taniguchi, James Hone, Cory Dean, Angel Rubio, and Abhay N. Pasupathy, “Maximized electron interactions at the magic angle in twisted bilayer graphene,” *Nature* **572**, 95–100 (2019).
- [36] Yonglong Xie, Biao Lian, Berthold Jäck, Xiaomeng Liu, Cheng-Li Chiu, Kenji Watanabe, Takashi Taniguchi, B. Andrei Bernevig, and Ali Yazdani, “Spectroscopic sig-

- natures of many-body correlations in magic-angle twisted bilayer graphene,” *Nature* **572**, 101–105 (2019).
- [37] Yuhang Jiang, Xinyuan Lai, Kenji Watanabe, Takashi Taniguchi, Kristjan Haule, Jinhai Mao, and Eva Y. Andrei, “Charge order and broken rotational symmetry in magic-angle twisted bilayer graphene,” *Nature* **573**, 91–95 (2019).
- [38] Dillon Wong, Kevin P. Nuckolls, Myungchul Oh, Biao Lian, Yonglong Xie, Sangjun Jeon, Kenji Watanabe, Takashi Taniguchi, B. Andrei Bernevig, and Ali Yazdani, “Cascade of transitions between the correlated electronic states of magic-angle twisted bilayer graphene,” arXiv e-prints , arXiv:1912.06145 (2019), [arXiv:1912.06145 \[cond-mat.mes-hall\]](#).
- [39] Uri Zondiner, Asaf Rozen, Daniel Rodan-Legrain, Yuan Cao, Raquel Queiroz, Takashi Taniguchi, Kenji Watanabe, Yuval Oreg, Felix von Oppen, Ady Stern, *et al.*, “Cascade of phase transitions and dirac revivals in magic angle graphene,” arXiv preprint arXiv:1912.06150 (2019).
- [40] Petr Stepanov, Ipsita Das, Xiaobo Lu, Ali Fahimniya, Kenji Watanabe, Takashi Taniguchi, Frank HL Koppens, Johannes Lischner, Leonid Levitov, and Dmitri K Efetov, “The interplay of insulating and superconducting orders in magic-angle graphene bilayers,” arXiv preprint arXiv:1911.09198 (2019).
- [41] Yu Saito, Jingyuan Ge, Kenji Watanabe, Takashi Taniguchi, and Andrea F Young, “Decoupling superconductivity and correlated insulators in twisted bilayer graphene,” arXiv preprint arXiv:1911.13302 (2019).
- [42] Nick Bultinck, Eslam Khalaf, Shang Liu, Shubhayu Chatterjee, Ashvin Vishwanath, and Michael P. Zaletel, “Ground State and Hidden Symmetry of Magic Angle Graphene at Even Integer Filling,” arXiv e-prints , arXiv:1911.02045 (2019), [arXiv:1911.02045 \[cond-mat.str-el\]](#).
- [43] E. Suárez Morell, J. D. Correa, P. Vargas, M. Pacheco, and Z. Barticevic, “Flat bands in slightly twisted bilayer graphene: Tight-binding calculations,” *Phys. Rev. B* **82**, 121407 (2010).
- [44] J. M. B. Lopes dos Santos, N. M. R. Peres, and A. H. Castro Neto, “Continuum model of the twisted graphene bilayer,” *Phys. Rev. B* **86**, 155449 (2012).
- [45] Rafi Bistritzer and Allan H. MacDonald, “Moire bands in twisted double-layer graphene,” *Proceedings of the National Academy of Sciences* **108**, 12233–12237 (2011).
- [46] Hoi Chun Po, Liujun Zou, Ashvin Vishwanath, and T. Senthil, “Origin of mott insulating behavior and superconductivity in twisted bilayer graphene,” *Phys. Rev. X* **8**, 031089 (2018).
- [47] W. Kohn and J. M. Luttinger, “New mechanism for superconductivity,” *Phys. Rev. Lett.* **15**, 524–526 (1965).
- [48] Saurabh Maiti and Andrey V. Chubukov, “Superconductivity from repulsive interaction,” *AIP Conference Proceedings* **1550**, 3–73 (2013).
- [49] Jonathan Ruhman and Patrick A. Lee, “Superconductivity at very low density: The case of strontium titanate,” *Phys. Rev. B* **94**, 224515 (2016).
- [50] Vladyslav Kozii, Zhen Bi, and Jonathan Ruhman, “Superconductivity near a ferroelectric quantum critical point in ultralow-density dirac materials,” *Phys. Rev. X* **9**, 031046 (2019).
- [51] Maria N. Gastiasoro, Jonathan Ruhman, and Rafael M. Fernandes, “Superconductivity in dilute SrTiO₃: a review,” arXiv e-prints , arXiv:1912.01509 (2019), [arXiv:1912.01509 \[cond-mat.supr-con\]](#).
- [52] Jian Kang and Oskar Vafek, “Strong coupling phases of partially filled twisted bilayer graphene narrow bands,” *Phys. Rev. Lett.* **122**, 246401 (2019).
- [53] Yuan Da Liao, Jian Kang, Clara N. Breiø, Xiao Yan Xu, Han-Qing Wu, Brian M. Andersen, Rafael M. Fernandes, and Zi Yang Meng, “Correlation-induced insulating topological phases at charge neutrality in twisted bilayer graphene,” arXiv e-prints , arXiv:2004.12536 (2020), [arXiv:2004.12536 \[cond-mat.str-el\]](#).
- [54] Haruki Watanabe and Ashvin Vishwanath, “Criterion for stability of Goldstone modes and Fermi liquid behavior in a metal with broken symmetry,” *Proceedings of the National Academy of Science* **111**, 16314–16318 (2014).
- [55] Note that this equation is approximate since it relies on the assumption of an isotropic spectrum on the Fermi surface.
- [56] Yuan Cao, Daniel Rodan-Legrain, Jeong Min Park, Fanqi Noah Yuan, Kenji Watanabe, Takashi Taniguchi, Rafael M. Fernandes, Liang Fu, and Pablo Jarillo-Herrero, “Nematicity and Competing Orders in Superconducting Magic-Angle Graphene,” arXiv e-prints , arXiv:2004.04148 (2020), [arXiv:2004.04148 \[cond-mat.mes-hall\]](#).
- [57] Ming Xie and A. H. MacDonald, “Nature of the correlated insulator states in twisted bilayer graphene,” *Phys. Rev. Lett.* **124**, 097601 (2020).
- [58] Shang Liu, Eslam Khalaf, Jong Yeon Lee, and Ashvin Vishwanath, “Nematic topological semimetal and insulator in magic angle bilayer graphene at charge neutrality,” arXiv e-prints , arXiv:1905.07409 (2019), [arXiv:1905.07409 \[cond-mat.str-el\]](#).
- [59] Tommaso Cea and Francisco Guinea, “Band structure and insulating states driven by the Coulomb interaction in twisted bilayer graphene,” arXiv e-prints , arXiv:2004.01577 (2020), [arXiv:2004.01577 \[cond-mat.str-el\]](#).
- [60] Jian Kang and Oskar Vafek, “Non-Abelian Dirac node braiding and near-degeneracy of correlated phases at odd integer filling in magic angle twisted bilayer graphene,” arXiv e-prints , arXiv:2002.10360 (2020), [arXiv:2002.10360 \[cond-mat.str-el\]](#).
- [61] Yuan Da Liao, Zi Yang Meng, and Xiao Yan Xu, “Valence bond orders at charge neutrality in a possible two-orbital extended hubbard model for twisted bilayer graphene,” *Phys. Rev. Lett.* **123**, 157601 (2019).
- [62] Laura Classen, Carsten Honerkamp, and Michael M. Scherer, “Competing phases of interacting electrons on triangular lattices in moiré heterostructures,” *Physical Review B* **99** (2019), [10.1103/physrevb.99.195120](#).
- [63] Lennart Klebl, Dante M. Kennes, and Carsten Honerkamp, “Functional renormalization group for a large moiré unit cell,” arXiv e-prints , arXiv:2002.11030 (2020), [arXiv:2002.11030 \[cond-mat.str-el\]](#).
- [64] Jeil Jung, Ashley M. DaSilva, Allan H. MacDonald, and Shaffique Adam, “Origin of band gaps in graphene on hexagonal boron nitride,” *Nature Communications* **6**, 6308 (2015).
- [65] Hakseong Kim, Nicolas Leconte, Bheema L. Chittari, Kenji Watanabe, Takashi Taniguchi, Allan H. MacDonald, Jeil Jung, and Suyong Jung, “Accurate Gap Determination in Monolayer and Bilayer Graphene/h-BN Moiré Superlattices,” *Nano Letters* **18**, 7732–7741

- (2018).
- [66] A. A. Zibrov, E. M. Spanton, H. Zhou, C. Kometter, T. Taniguchi, K. Watanabe, and A. F. Young, “Even-denominator fractional quantum Hall states at an isospin transition in monolayer graphene,” *Nature Physics* **14**, 930–935 (2018).
- [67] Matthew Yankowitz, Jeil Jung, Evan Laksono, Nicolas Leconte, Bheema L. Chittari, K. Watanabe, T. Taniguchi, Shaffique Adam, David Graf, and Cory R. Dean, “Dynamic band-structure tuning of graphene moiré superlattices with pressure,” *Nature* **557**, 404–408 (2018).
- [68] Liujun Zou, Hoi Chun Po, Ashvin Vishwanath, and T. Senthil, “Band structure of twisted bilayer graphene: Emergent symmetries, commensurate approximants, and wannier obstructions,” *Phys. Rev. B* **98**, 085435 (2018).
- [69] Nick Bultinck, Shubhayu Chatterjee, and Michael P. Zaletel, “Anomalous Hall ferromagnetism in twisted bilayer graphene,” arXiv e-prints, arXiv:1901.08110 (2019), [arXiv:1901.08110 \[cond-mat.str-el\]](https://arxiv.org/abs/1901.08110).
- [70] Ya-Hui Zhang, Dan Mao, and T. Senthil, “Twisted bilayer graphene aligned with hexagonal boron nitride: Anomalous Hall effect and a lattice model,” *Phys. Rev. Research* **1**, 033126 (2019).
- [71] Hilbert v. Löhneysen, Achim Rosch, Matthias Vojta, and Peter Wölfle, “Fermi-liquid instabilities at magnetic quantum phase transitions,” *Rev. Mod. Phys.* **79**, 1015–1075 (2007).
- [72] G. R. Stewart, “Non-Fermi-liquid behavior in d - and f -electron metals,” *Rev. Mod. Phys.* **73**, 797–855 (2001).
- [73] Vadim Oganesyan, Steven A. Kivelson, and Eduardo Fradkin, “Quantum theory of a nematic Fermi fluid,” *Phys. Rev. B* **64**, 195109 (2001).
- [74] W. Metzner, D. Rohe, and S. Andergassen, “Soft Fermi surfaces and breakdown of Fermi-liquid behavior,” *Phys. Rev. Lett.* **91**, 066402 (2003).
- [75] Ar. Abanov and Andrey V. Chubukov, “Spin-fermion model near the quantum critical point: One-loop renormalization group results,” *Phys. Rev. Lett.* **84**, 5608–5611 (2000).
- [76] Max A. Metlitski and Subir Sachdev, “Quantum phase transitions of metals in two spatial dimensions. I. Ising-nematic order,” *Phys. Rev. B* **82**, 075127 (2010).
- [77] Max A. Metlitski and Subir Sachdev, “Quantum phase transitions of metals in two spatial dimensions. II. Spin density wave order,” *Phys. Rev. B* **82**, 075128 (2010).
- [78] Sung-Sik Lee, “Recent developments in non-Fermi liquid theory,” *Annual Review of Condensed Matter Physics* **9**, 227–244 (2018).
- [79] Zhida Song, Zhijun Wang, Wujun Shi, Gang Li, Chen Fang, and B. Andrei Bernevig, “All magic angles in twisted bilayer graphene are topological,” *Phys. Rev. Lett.* **123**, 036401 (2019).
- [80] Kasra Hejazi, Chunxiao Liu, Hassan Shapourian, Xiao Chen, and Leon Balents, “Multiple topological transitions in twisted bilayer graphene near the first magic angle,” *Phys. Rev. B* **99**, 035111 (2019).
- [81] S. Lederer, Y. Schattner, E. Berg, and S. A. Kivelson, “Enhancement of superconductivity near a nematic quantum critical point,” *Phys. Rev. Lett.* **114**, 097001 (2015).
- [82] Kenneth G. Wilson and Michael E. Fisher, “Critical exponents in 3.99 dimensions,” *Phys. Rev. Lett.* **28**, 240–243 (1972).